HORMONAL HOMEOSTASIS TO MITIGATE FEMALE HORMONE DISORDER: A COMPUTATIONAL APPROACH

M.Sc. Thesis

2024

For partial fulfilment of the requirements for

the Master of Science in Biotechnology

Submitted to

Central Department of Biotechnology

Tribhuvan University

Kirtipur, Kathmandu, Nepal

Submitted by

Aashish Pokharel

Roll No: BT 601/075

TU Regd No: 5-2-282-309-2014

HORMONAL HOMEOSTASIS TO MITIGATE FEMALE HORMONE DISORDER: A COMPUTATIONAL APPROACH

M.Sc. Thesis

2024

For partial fulfilment of the requirements for

the Master of Science in Biotechnology

Submitted to

Central Department of Biotechnology

Tribhuvan University

Kirtipur, Kathmandu, Nepal

Submitted by

Aashish Pokharel

Roll No: BT 601/075

TU Regd No: 5-2-282-309-2014

Supervisor

Dr. Pramod Aryal

Senior Scientist

Central Department of Biotechnology

Tribhuvan University

Kirtipur, Kathmandu, Nepal

Tribhuvan University
CENTRAL DEPARTMENT OF BIOTECHNOLOGY
Kirtipur, Kathmandu, Nepal

Date: 22 April 2024

Recommendation

This is to certify that the research work entitled **"HORMONAL HOMEOSTASIS TO MITIGATE FEMALE HORMONE DISORDER: A COMPUTATIONAL APPROACH"** has been carried out by Mr. Aashish Pokharel under my supervision.

This thesis work was performed for the partial fulfillment of the Master of Science in Biotechnology under the course code BT 621. The result presented here is his original findings. I hereby recommend this thesis for final evaluation.

Dr. Pramod Aryal
(Supervisor)
Central Department of Biotechnology
Tribhuvan University
Kirtipur, Kathmandu
Nepal

Tribhuvan University

CENTRAL DEPARTMENT OF BIOTECHNOLOGY

Kirtipur, Kathmandu, Nepal

Date: 22 April 2024

Certificate of Evaluation

This is to certify that the thesis entitled **"HORMONAL HOMEOSTASIS TO MITIGATE FEMALE HORMONE DISORDER: A COMPUTATIONAL APPROACH"** presented to evaluation committee by Mr. Aashish Pokharel is found satisfactory for the partial fulfillment of Master of Science in Biotechnology.

Prof. Dr. Krishna Das Manandhar
(Head of Department)
Central Department of Biotechnology
Tribhuvan University
Kirtipur, Kathmandu
Nepal

Prof. Dr. Narayan Adhikari
(External Examiner)
Central Department of Physics
Tribhuvan University
Kirtipur, Kathmandu
Nepal

Dr. Preeti Regmi
(Internal Examiner)
Central Department of Biotechnology
Tribhuvan University
Kirtipur, Kathmandu
Nepal

Dr. Pramod Aryal
(Supervisor)
Central Department of Biotechnology
Tribhuvan University
Kirtipur, Kathmandu
Nepal

Acknowledgement

I would like to extend my heartfelt gratitude to Dr. Pramod Aryal, my esteemed supervisor and mentor, whose unwavering guidance and support have been invaluable throughout my journey towards completing my master's thesis. His insightful feedback, patience, and encouragement have played a pivotal role in shaping my research and academic growth. Oreover, he has not only imparted knowledge but has also instilled in me a profound appreciation for the essence and significance of science. Through his mentorship, I have learned not only about the technical aspects of my field but also about the ethos and integrity that underpin scientific inquiry. I am deeply grateful for Dr. Pramod Aryal's continuous support, which has been instrumental in shaping my academic and professional journey.

I am also thankful to Prof. Dr. Rajendra Prashad Koirala, Central Department of Physics, Tribhuvan University for providing me with his valuable insight about the technology of molecular dynamics simulation.

I am also thankful to Prof. Dr. Rajendra Adhikari, Department of Physics, Kathmandu University for providing me with the computational resources and guidance in running simulation under his guidance.

I am also thankful to Prof Dr. Krishna Das Manandhar, HOD of Central Department of Biotechnology, Tribhuvan University for letting me complete my thesis works at TU.

Sincere thanks to my colleagues Ms. Alisha Nepali, Ms. Pooja Shrestha, Ms. Binita Khadka, Ms. Jeshika Thapa, Ms. Ashmita Aryal and Ms, Sujata Pokhrel for their noble contributions and assistance in my thesis works.

I would also like to acknowledge my seniors Mr. Samiran Subedi, Ms. Kabita Kandel, Mr. Siddhartha Gautam for assisting me during a time of need. I would also like to thanks my junior Sandesh Prasad Koirala, Bhawana Samal Magar, Amit Kumar Yadav, Anisha Regmi, Renu Kunwar, Sanjeeta Napit from Department of Biotechnology, SANN International College for assisting me with the necessary works over the course of my thesis work.

Last but not the least, I must express my profound gratitude to my parents for providing me continued help and support throughout all these years and through the process of research works and writing this thesis.

Thanks for all your encouragement!!!

Aashish Pokharel

Registration No: 5-2-282-309-2014

List of abbreviations

ADME	Absorption, Disposition, Metabolism And Excretion
APC	Adenomatous Polyposis Coli
CADD	Computer Aided Drug Discovery
CK1	Casein Kinase 1
CREB	Camp Response Element-Binding Protein
DAAM1	DVL-Associated Activator Of Morphogenesis 1
DEP	Dishevelled, Egl-10, Pleckstrin
DFT	Density Functional Computations
DIX	Dishevelled And Axin
DVL	Dishevelled
ERK	Extracellular Signal-Regulated Kinase
FDA	Food And Drug Administration
FGF-R1	Fibroblast Growth Factor Receptor–1
FSH	Follicle Stimulating Hormone
FZD	Frizzled
GDP	Guanosine Diphosphate
GnRH	Gonadotropin Releasing Hormone
GSK3	Glycogen Synthase Kinase 3
GUI	Graphical User Interface
HCG	Human Chorionic Gonadotropin
HOMO	Highest Occupied Molecular Orbital
HTS	High Throughput Screening
LBDD	Ligand Based Drug Design
LH	Luteinizing Hormone
LOMO	Lowest Occupied Molecular Orbital
LRP 5/6	Low Density Lipoprotein Receptor Related Protein 5/6
MAP	Mitogen Activated Protein Kinase
MAT	Methionine Adenosyltransferase
MEP	Molecular Electrostatic Potential Maps
mTOR	Mammalian Target Of Rapamycin
NMR	Nuclear Magnetic Resonance

NSAIDs	Nonsteroidal Anti-Inflammatory Drugs
OSIRIS	Open-Source Independent Review And Interpretation System
PAF	Platelet Activating Factor
PCP	Planar Cell Polarity
PDB	Protein Data Bank
PDBQT	Protein Data Bank, Partial Charge (Q), And Atom Type (T)
PDZ	Post Synaptic Density-95/Discs Large/Zonula- Occludens-1
PGE2	Prostaglandin E2
PKA	Protein Kinase A
PKC	Protein Kinase C
PLC	Phospholipase C
PP2A	Protein Phosphatase 2a
RCSB	Research Collaboratory For Structural Bioinformatics
Rhob	Ras Homolog Family Member
RIT	Ritonavir
SAM	S-Adenosylmethionine
SAR	Structure-Activity Relationship
SAS	Statistical Analysis System
SBDD	Structure Based Drug Design
SF-1	Steroidogenic Factor-1
TCF	Transcription Factor
TNF	Tumor Necrosis Factor
TPSA	Topological Polar Surface Area
UCSF	University Of California, San Francisco's Department Of Pharmaceutical Chemistry
UFF	Universal Force Field
VS	Virtual Screening

List of tables

List of figures

Table of Content

Abstract

In this research, PORCN, DVL, and AXIN were prioritized as key proteins regulating the Wnt/beta-catenin signaling pathway, estrogen regulation, and cell proliferation. Maintaining the expression and regulation of these proteins is crucial for controlling estrogen production, providing a therapeutic target. Computer-Aided Drug Design (CADD) was employed to develop novel disease-containment medication candidates. By using an optimized protocol for protein identification and improved practices in the selection of drug compounds, including their metabolic profiling, comprehensive data coverage was achieved. As part of our computational drug discovery approach, we searched for compounds or ligands (both natural products and biogenic) in the ZINC 15 database. The ligands were filtered for ADME/TOX properties, followed by additional filtering with hMAT1A and CYP3A4, along with other Phase I drug-metabolizing enzymes. Protein-ligand interactions of top hits with aromatase were analyzed, and further Density Functional Theory (DFT) analysis was performed to support the molecular docking results. Based on their inability to inhibit SAM biosynthesis and cytochromes, binding energy, stability of molecular interactions, and the energy gap between molecular orbital stages, the following compounds were identified as potential lead compounds: 42151 (biogenic), 31802, 1765, and 6753. These compounds showed promise against the PORCN, PDZ, DEP, and DIX domains of DVL, and the DIX domain of AXIN, respectively.

Keywords: CADD, ADME/TOX, PORCN, DVL, AXIN, Wnt/beta-catenin signaling pathway, Estrogen regulation, Cell proliferation, Phase I drug-metabolizing enzymes, Density Functional Theory (DFT)

CHAPTER 1

INTRODUCTION

1.1Background

Uterine fibroids, also known as myomas, are benign monoclonal tumors in the uterus, influenced by estrogens and progestogens. They are uncommon before menarche and tend to shrink post-menopause, highlighting hormonal involvement in their growth. As the most prevalent benign tumors in women and a major cause of hysterectomies in the USA, fibroids lack comprehensive epidemiological data due to inconsistent study populations and screening methods, complicating the comparison of existing research.

The prevalence of uterine fibroids varies widely, ranging between 5% and 21%. A U.S. study of women aged 35 to 49, using self-reporting, medical records, and sonography, revealed that 60% of African-American women had fibroids by age 35, increasing to over 80% by age 50. For Caucasian women, the prevalence was 40% by age 35 and nearly 70% by age 50. Despite this high prevalence, uterine fibroids often remain undetected due to asymptomatic presentations, resulting in limited medical attention.

When symptoms do occur, they commonly include heavy and prolonged uterine bleeding, particularly "gushing" bleeding and increased use of pads or tampons. According to Wegenka et al. (2004), women with fibroids are more likely to experience these symptoms, along with dyspareunia and non-cyclic pelvic pain. However, systematic research on fibroid symptoms remains scarce, highlighting the need for further investigation into the clinical presentation and impact of this condition.

To manage these symptoms, various treatments for myomas include medical therapies, surgery, and uterine artery embolization. While oral contraceptives and progestins are commonly used to manage bleeding despite limited evidence of their efficacy in treating myomas, other options like levonorgestrel-releasing intrauterine systems (LNG-IUS) and GnRH agonists are also available. However, LNG-IUS is unsuitable for severe uterine cavity distortion, and GnRH agonist use is restricted due to hypoestrogenic side effects. Surgical procedures such as myomectomy, endometrial ablation, and hysterectomy are chosen based on symptom severity and reproductive goals, with possible side effects including uterine hemorrhage, headache, ovarian cysts, vaginitis, dysmenorrhea, and breast discomfort.

While traditional medical and surgical interventions, along with uterine artery embolization, have proven effective for managing symptoms, the lack of supportive evidence for oral contraceptives underscores the need for more targeted treatments. In this context, computer-aided drug discovery (CADD) emerges as a pivotal tool in advancing new drug development. CADD excels in identifying target compounds, elucidating their mechanisms, and validating their research relevance. Chemoinformatics further enhances in silico drug design by integrating diverse data sources, ensuring research accuracy and efficacy. These tools play a crucial role in identifying and prioritizing compounds, reducing lead compound rejection, and aiding high-throughput screening (HTS), thereby demonstrating their instrumental role in discovering hit compounds.

In drug development, high-throughput screening (HTS) is traditionally used to identify lead compounds by testing large libraries against a target. However, computational methods like computer-aided drug design (CADD) have revolutionized the process. By employing virtual screening and receptor-based techniques, CADD significantly streamlines lead discovery by predicting molecular interactions, thus prioritizing compounds with high binding potential. This advancement complements HTS by streamlining the identification of lead compounds against specific targets.

Structure-based drug design (SBDD) and ligand-based drug design (LBDD) are leading approaches in computer-aided drug design (CADD). SBDD involves analyzing macromolecule 3D structures and docking ligands for potential drug candidates, ensuring tight binding to active sites and meeting ADMET criteria. Conversely, LBDD relies on structural similarity, assuming molecules with akin structures have analogous biological functions and bind similarly. Key considerations for defining target compounds include druggability, molecular flexibility, protonation state, and water molecule interactions. Ultimately, compound effectiveness hinges on their pharmacokinetic and ADMET properties, aligning with the goals of modern drug development (Cerqueira et al., 2009).

The foundation laid by the Human Genome Project has revolutionized drug discovery, providing a vast repertoire of therapeutic targets. Leveraging advanced protein purification techniques, such as high-throughput methods and crystallography, enhances the understanding of target structures. (Meng et al., 2012). In this context, molecular docking emerges as a pivotal tool, facilitating the efficient screening of ligands and targets by predicting their interactions. By integrating criteria like binding energy, programs like AutoDock and PyRx aid in the

selection of promising drug candidates (Sgobba et al., 2012; Hernández-Santoyo et al., 2013). This process, bolstered by protein structures sourced from databases like RCSB, streamlines drug discovery efforts, including both novel compound identification and repurposing initiatives (March-Vila et al., 2017; Hernández-Santoyo et al., 2013).

1.2 Hypothesis

1.2.1 Null hypothesis:

Potential lead compound showed no significant reaction against the prioritized target proteins regulating, hormonal disorders in female.

1.2.2 Alternate hypothesis

Potential lead compound showed significant reaction against the prioritized target proteins regulating, hormonal disorders in female.

1.3 Objectives

1.3.1 General objective:

1. To develop potential lead compounds, capable of mitigating hormonal disorder in females.

1.3.2 Specific objectives:

2. To identify drug target necessary for disease etiology
3. To create ligand library screening with stringent parameters of druggability.
4. To perform molecular docking and analyzing the protein interactions.
5. To study protein ligand interaction
6. To choose probable drug candidates
7. To perform DFT computation to analyze electrochemical properties if selected drug candidate
8. To perform and analyze molecular dynamic simulation.

CHAPTER 2

LITERATURE REVIEW

2.1 Menstruation

Women typically experience a reproductive period spanning around 36 years, from the onset of menstruation (usually between 8.5 to 13 years) to menopause at around 51 (Aydos et al., 2005; Harlow, 2000; Park et al., 2002). Puberty, lasting approximately 2.3 years, progresses through stages including breast development, growth of pubic and axillary hair, and culminates in menarche, the onset of menstruation (Park et al., 2002; Mihm et al., 2011).

2.1.1 The Menstrual Cycle: Overview

The menstrual cycle, governed by a complex interplay of hormonal mechanisms, orchestrates ovarian follicular development, ovulation, luteinization, luteolysis, and endometrial remodeling. These processes sustain reproductive functions from puberty to menopause (Mihm et al., 2011).

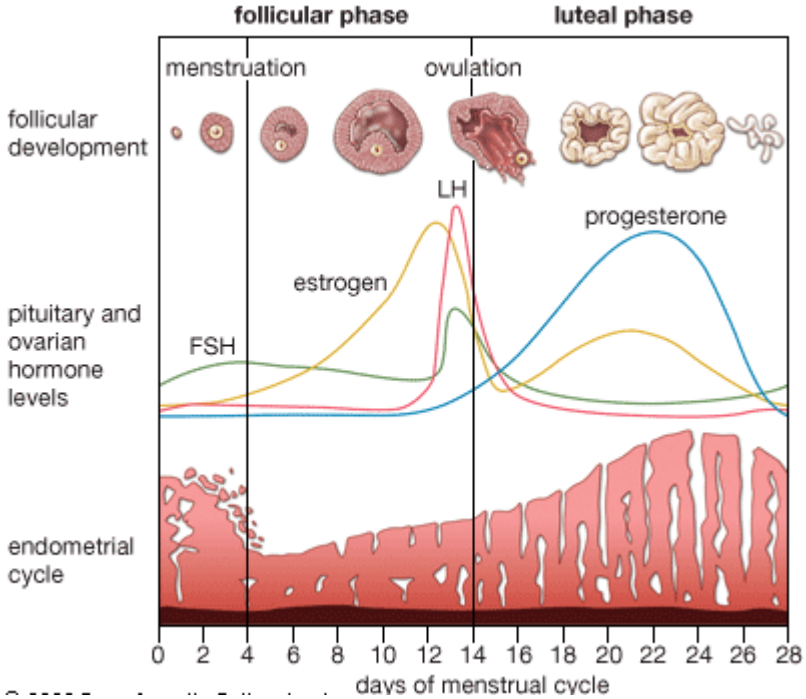

Fig 1: Cyclical changes during a woman's normal ovulatory menstrual cycle (Clayton, S. George, 2024)

The menstrual cycle consists of four main phases:

- The follicular phase (Days 1-14),

- Ovulation (Day 14),
- The luteal phase (Days 14-28), and
- Menstruation (Days 0-5).

During the follicular phase, estrogen regulates the growth of the endometrial layer and prepares the uterus for potential implantation, while also influencing cervical mucus to facilitate sperm entry (Herbison, 2020).

Ovulation occurs around Day 14 when luteinizing hormone (LH) surges, triggering the release of a mature egg from the follicle. The luteal phase, initiated by LH, sees progesterone becoming the dominant hormone, secreted by the corpus luteum formed from the ruptured follicle. Progesterone prepares the endometrium for implantation by enhancing mucous secretions and vascular supply. Concurrently, declining estrogen levels lead to increased cervical mucus, hindering sperm entry (Herbison, 2020).

Finally, menstruation begins as hormone levels drop at the end of the luteal phase, resulting in the shedding of the endometrial layer. Menstrual flow, occurring between Days 0-5 of the next cycle, comprises arterial blood fortified with various components, with its duration and intensity influenced by factors like blood disorders, endometrial thickness, and medication usage (Thiyagarajan, Basit, & Jeanmonod, 2022).

The menstrual cycle, with its intricate hormonal interplay, serves to prepare the uterus for potential conception and maintain reproductive health (Thiyagarajan, Basit, & Jeanmonod, 2022). This cyclical process culminates in menstrual bleeding, marking the transition between the luteal and follicular phases (Critchley et al., 2020). Lasting typically 3-6 days, menstrual bleeding varies in volume and duration among individuals, with an average blood loss of 33.2 ml on Day 2 (Mihm et al., 2011). Despite these variations, normal menstruation is characterized by the cyclic shedding of the uterine lining throughout a woman's reproductive years, encompassing the frequency, regularity, duration, and volume of bleeding episodes (Critchley et al., 2020).

2.2 Any Deviation from Regular Menstrual Cycle

The average menstrual cycle typically spans 21 to 35 days, with menstrual bleeding lasting for approximately seven days (Critchley et al., 2020). It is noteworthy that menstrual flow is typically heaviest during the initial days of bleeding, gradually diminishing towards the end of the cycle (Critchley et al., 2020).

While factors such as age, ethnicity, and socioeconomic status influence variations in menstrual phases and blood volume (Mihm et al., 2011), it's crucial to acknowledge that not all women conform to this standard pattern. Deviations from the norm in menstrual cycles are common, highlighting the diverse nature of women's reproductive health experiences. Menstrual irregularities often include:

Dysmenorrhea (Painful Cramps)

Dysmenorrhea, which is characterized by severe, frequent cramps primarily in the lower abdomen, but may also extend to the lower back and thighs. Dysmenorrhea is classified into two types: primary dysmenorrhea, which arises from uterine contractions during menstruation, and secondary dysmenorrhea, which is linked to underlying medical conditions such as endometriosis or uterine fibroids.

Menorrhagia (Heavy Bleeding)

Menorrhagia refers to abnormally heavy and prolonged menstrual bleeding, exceeding 7 days and involving more than 5 sanitary product changes per day, including at night. Women may pass large clots and experience painful cramping (dysmenorrhea) due to the excessive bleeding, which significantly surpasses the typical 1 ounce (30 mL) blood loss of a normal menstrual cycle.

Abnormal uterine bleeding encompasses several conditions. Menorrhagia involves excessively heavy or prolonged menstrual bleeding. Metrorrhagia refers to irregular bleeding episodes between periods or unrelated to the menstrual cycle, often seen at the onset of menstruation or during ovulation. Menometrorrhagia combines characteristics of menorrhagia and metrorrhagia, with heavy, prolonged, and irregular bleeding. Dysfunctional uterine bleeding (DUB) results from hormonal imbalances, particularly anovulation, leading to excessive or irregular bleeding, commonly occurring during puberty or menopause. Other forms include postcoital bleeding and postmenopausal bleeding, the latter of which can indicate serious health issues.

Amenorrhea (Absence of Menstruation)

Amenorrhea, the absence of menstruation, is divided into primary and secondary categories. Primary amenorrhea is diagnosed if menstruation hasn't begun by age 16, with earlier evaluation recommended for girls with no signs of puberty by 13 or no period by 15. Secondary amenorrhea is defined as the cessation of previously regular periods for at least three months.

2.3 Epidemiological Studies

2.3.1 International studies

The study conducted by Ravi et al. (2016) highlights the prevalence of menstrual issues among adolescent girls. The average age of the participants was 14.74 years, with menarche typically occurring at 12.4 years. A significant 87.7% of the girls reported experiencing some form of menstrual problem. Specifically, 72.6% of the participants suffered from dysmenorrhea, 45.7% had menorrhagia, and 31.7% experienced irregular menstrual cycles.

Similarly, a hospital-based observational study at S. P. Medical College, Bikaner, Rajasthan, examined the bleeding patterns in 100 patients attending the Gynecology OPD. The study found that menorrhagia was the most prevalent form of Abnormal Uterine Bleeding (AUB), affecting 49% of the cases. Metrorrhagia was the next most common, observed in 26% of the cases. The socioeconomic status of the patients showed that 70% were from the Above Poverty Line (APL) category, while 30% belonged to the Below Poverty Line (BPL) category (Maharia & Garg, 2020).

Further adding to the understanding of menstrual issues among adolescents, a study conducted in Italy provided a different perspective. In this study, the occurrence rates of various menstrual disorders among the adolescent population were as follows: Dysmenorrhea at 6.2%, Polymenorrhea at 3%, Oligomenorrhea at 3.4%, Hypomenorrhea at 3.2%, Menorrhagia at 19%, and irregular menstrual cycles at 9% (Rigon et al., 2012).

2.3.2 National Studies

Chapagain and Dangal (2020) conducted a prospective cross-sectional study at Paropakar Maternity and Women's Hospital in Kathmandu over one year, examining 77 perimenopausal women with abnormal uterine bleeding. The study revealed that the most common age group among these women was 40 to 44 years. Menorrhagia was the predominant clinical feature (40.3%), followed by menometrorrhagia (23.4%). The majority of these women were multiparous, with a parity of 3 to 4 (49.4%). Histopathological analysis showed that the most common finding was proliferative endometrium (37.7%), followed by secretory endometrium (31.2%). Proliferative endometrium was associated with menorrhagia and menometrorrhagia, while secretory endometrium was linked to metrorrhagia.

Complementing these findings, a factor analysis of data from 4,828 women revealed a single factor model indicating heavy menstrual bleeding. In this pooled sample, 48.6% of women

were classified as experiencing heavy menstrual bleeding, with the lowest prevalence in Dakar (38.3%) and Kampala (38.4%), and the highest in Kathmandu (77.6%). Heavy menstrual bleeding was significantly linked to symptoms such as fatigue or shortness of breath during menstruation and poorer self-rated physical health (Sinharoy et al., 2023).

In Kathmandu, Nepal, where cultural taboos surrounding menstruation are prevalent, the highest occurrence of heavy menstrual bleeding (77.6%) was observed. This high prevalence may be exacerbated by negative perceptions of menstruation. The subjective nature of heavy bleeding experiences suggests that various sociocultural, environmental, and individual factors contribute to the variability observed in the study (Sinharoy et al., 2023).

Further supporting the prevalence of menstrual abnormalities, a study conducted by Shrestha DN et al. (2017) over 427 females of reproductive age (15-49 years) found that 23.4% reported menstrual abnormalities. Among these, 21.7% complained of menorrhagia. This aligns with the findings from Chapagain and Dangal (2020), highlighting menorrhagia as a significant clinical feature among women with menstrual abnormalities in the region.

These studies collectively underscore the significant prevalence of menstrual disorders across different populations and settings, highlighting the need for greater attention to menstrual health in adolescent girls.

2.4 Effect Of Menorrhagia In Quality Of Women’s Life

According to the World Health Organization, "health" is defined as "a state of complete physical, mental, and social well-being and not merely the absence of disease or infirmity." For women, menstrual health is a crucial component of overall health because, between menarche and menopause, most women experience menstruation, which significantly influences their physical, mental, and social well-being (Critchley et al., 2020).

Disturbances in menstrual patterns can impact both physical and psychological health, ultimately affecting the quality of life for women (Dhar et al., 2023). Quality of life relates to how individuals perceive their life circumstances in relation to their goals, expectations, and cultural values. Although menorrhagia is typically not life-threatening, it substantially affects women's personal, social, familial, and occupational spheres, thereby reducing their overall well-being. Often, women are more concerned with the disruption of daily activities than the actual volume of bleeding (Gokyildiz et al., 2013).

Heavy menstrual bleeding is linked to several adverse functional outcomes, such as decreased productivity, lower income, reduced ability to perform daily activities, and limitations on social life and relationships (Sinharoy et al., 2023). This condition profoundly affects various aspects of a woman's quality of life, including energy levels, mood, work productivity, social interactions, family life, and sexual functioning. The negative impact on quality of life for women with heavy menstrual bleeding also stems from the clinical consequences of prolonged, excessive blood loss. Persistent heavy bleeding depletes iron stores and circulating iron levels, leading to iron deficiency and ultimately iron-deficiency anemia (Fraser et al., 2015).

Menorrhagia is a major contributor to iron deficiency and iron deficiency anemia, both of which have detrimental effects on women's health. This condition leads to increased consultations with gynecology departments, hospitalizations, and surgeries (Gokyildiz et al., 2013).

2.5 Causes of Menorrhagia

Menorrhagia, now commonly referred to as abnormal uterine bleeding (AUB), is classified into structural and non-structural causes using the PALM-COEIN acronym: Polyp, Adenomyosis, Leiomyoma, Malignancy and hyperplasia, Coagulopathy, Ovulatory dysfunction (e.g., due to hypothyroidism, hyperthyroidism, prolactin-secreting tumors, PCOS), Endometrial, Iatrogenic (e.g., IUDs, chemotherapeutic agents, anticoagulants), and Not yet classified. Proper identification of the underlying cause is crucial for effective management of AUB in women (Thiyagarajan, Basit, & Jeanmonod, 2022).

Menorrhagia, characterized by excessive menstrual bleeding, stems from a complex interplay of hormonal, mechanical, and clotting abnormalities (Livdans-Forret et al., 2007). While hormonal factors like anovulation and hypothyroidism contribute significantly, mechanical causes such as cancer and endometriosis also play a role. Moreover, clotting abnormalities like vitamin K deficiency exacerbate the disorder.

A systematic review focusing on heavy menstrual bleeding (HMB) among adolescents aged 10-19 found that over 40% of cases had no identifiable cause (Hall et al., 2024). Among those with identifiable causes, ovarian uterine disorders, coagulation disorders, and platelet disorders were the most prevalent systemic disorders, with respective prevalence percentages of 23.7%, 19.4%, and 6.23%. However, the PALM-COEIN classification system, while useful for

organizing HMB causes, lacks prior probabilities for each cause and struggles to estimate cases with unidentified etiologies.

2.6 Treatment of Menorrhagia

In managing pelvic issues like pelvic inflammatory disease or endometriosis, treatment options vary, with a preference for medical therapy in cases without evident pelvic abnormalities and a desire to preserve fertility (Rees, 1987). Surgical intervention may become necessary if medical treatment fails or in specific conditions, although a conservative approach is advised, particularly for women aiming to retain fertility (Rees, 1987).

2.6.1 Medical treatment

For effective management of menorrhagia, various medical treatments are available. Antifibrinolytic medicines and prostaglandin synthetase inhibitors like mefenamic acid are commonly prescribed during menstruation to reduce blood loss. Progestogens such as norethisterone can also lessen menstrual bleeding, especially during the luteal phase, though their impact on reducing blood loss is not conclusively proven. Oral contraceptives offer dual benefits for women under 35 requiring contraception. Clomiphene may be used to induce ovulation in cases of menorrhagia stemming from anovulation, but its effectiveness in reducing blood loss is uncertain, making it advisable to reserve for those aiming to conceive. Regular use of danazol can significantly reduce menstrual blood loss and may even lead to amenorrhea, crucial for addressing the risk of iron deficiency anemia associated with menorrhagia (Rees, 1987).

2.6.2 Surgical treatment

In terms of surgical interventions for menorrhagia, options include the removal of cervical or endometrial polyps, curettage, myomectomy, and hysterectomy. Endometrial polyps and sub-mucous fibroids can be excised using hysteroscopic management in specialized centers. While dilatation and curettage can temporarily reduce menstrual blood flow, its long-term impact on blood loss remains unclear, often viewed more as a diagnostic procedure than a definitive treatment. Hysterectomy is more commonly recommended for younger women who have completed their families, as older women can often manage menorrhagia with medications until menopause (Rees, 1987).

2.7 Uterine Fibroids

Uterine fibroid lesions, initially dubbed as "uterine stones" and later referred to as scleromas in the second century AD, have been historically recognized as benign neoplasms arising from the myometrium of the uterus (Yang et al., 2022). Commonly known as fibroids or myomas, these uterine leiomyomas typically manifest during pre- or peri-menopause, affecting 70–80% of women by age 50 (Wong et al., 2016; Tadir et al., 2008). They present a heterogeneous composition and variable size within individuals and among women. Notably, each fibroid is encapsulated by a fibro-neurovascular structure, distinguishing it from the surrounding normal myometrium (Tadir et al., 2008; Wong et al., 2016). Symptoms associated with fibroids include abnormal uterine bleeding, pelvic discomfort, and reproductive dysfunction, categorizing their impact into three distinct domains (Wong et al., 2016; Tadir et al., 2008).

Uterine fibroids, although typically non-cancerous, pose considerable health challenges, often necessitating hysterectomy and leading to various gynecologic and reproductive issues such as heavy menstrual bleeding, pelvic pain, and infertility. These complications contribute to a substantial economic burden on society, with estimated annual healthcare costs in the USA reaching approximately $34 billion (Tadir et al., 2008; Yang et al., 2022).

2.8 Fibroid Origins and Genesis

Recent studies suggest that uterine fibroids originate from stem cells within the myometrium, the muscular wall of the uterus composed of smooth muscle fibers and connective tissue. Although the precise cell of origin remains unidentified, evidence supports this hypothesis. Stem cells derived from both the myometrium and uterine fibroids have been isolated, and tumor-initiating cells within fibroids have been identified, further underlining the role of myometrial stem cells in fibroid development (Yang et al., 2022).

2.8.1 Wnt Signalling and Leiomyoma Stem Cell Biology

Uterine leiomyomas (UL) are believed to originate from stem cells within the myometrium, particularly a subset known as side population (SP) cells, which express stemness markers like OCT4, NANOG, DNMT3B, and GDF-3. These SP cells exhibit genetic and epigenetic abnormalities compared to myometrial cells and activate the Wnt/β-catenin pathway, crucial in UL development (El Sabeh et al., 2021).

Embryologic studies support the involvement of the Wnt/β-catenin pathway in UL, where constitutive overexpression of active β-catenin in mice led to myometrial hyperplasia

progressing into UL-like tumors. Furthermore, studies in female mice with selectively deleted β-catenin displayed a reduction in uterine size, suggesting the pathway's role in UL development (El Sabeh et al., 2021).

Despite relying on estrogen and progesterone for growth, leiomyoma SP cells exhibit low expression of their receptors. Nevertheless, they serve as tumor-initiating cells, interacting with mature myometrial cells via the Wnt/β-catenin pathway to promote growth. Hormone-induced nuclear translocation of β-catenin in leiomyoma SP cells, facilitated by mature myometrial cells, drives proliferation, emphasizing the importance of paracrine signaling in UL development (Ono et al., 2013).

2.8.2 Wnt pathway and uterine fibroids in relation with estrogen

The Wnt/β-catenin signaling pathway holds pivotal significance in various physiological processes, encompassing development, tissue renewal, cell proliferation, differentiation, and tumorigenesis (Yang et al., 2022). Recent investigations into its involvement in uterine fibroid formation have unveiled conflicting findings regarding the expression of β-catenin. While some studies indicate upregulated expression, others observe no discernible difference compared to the myometrium (Thakur, R., & Mishra, D. P., 2013; Zaitseva et al., 2013)

Notably, mislocalization of β-catenin, particularly its heightened nuclear presence in fibroids versus normal myometrium, has been associated with the fibroid phenotype. Studies suggest that estrogen induces β-catenin nuclear translocation and enhances its responsive gene expression in fibroid cells through the estrogen receptor (ER) (Ulin et al., 2020). This implies a paracrine role for the Wnt/β-catenin pathway in fostering fibroid growth, facilitating mature myometrium or fibroid cells to emit mitogenic signals to neighboring tissue stem cells in response to estrogen and progesterone (Ono et al., 2013s).

Moreover, Vitamin D3 has emerged as a potential inhibitor of this pathway, exhibiting the capability to diminish uterine fibroid cell proliferation (Al-Hendy et al., 2016). Encouragingly, β-catenin inhibitors such as ICG-001, cordycepin, and XAV939 have shown promise in mitigating these effects, offering avenues for therapeutic intervention (Corachán et al., 2019).

2.8.3 Synthesis of Estrogen in Leiomyoma tissue *In-situ*

The synthesis of estrogen within leiomyoma tissue has been extensively investigated since 1984, revealing elevated aromatase activity compared to normal myometrium, leading to increased concentrations of estrone and estradiol. Smooth muscle cells within leiomyoma

tissue contribute significantly to this activity, alongside altered levels of 17b-hydroxysteroid dehydrogenases (17b-HSDs) which interconvert estrone and estradiol. Moreover, leiomyoma exhibits estrone sulfatase activity, potentially influencing its growth, particularly during therapeutic interventions. This higher estrogen concentration in leiomyoma tissue compared to normal myometrium suggests a crucial role in leiomyoma pathogenesis and therapeutic response (Shozu et al., 2004).

2.8.3.1 Aromatase's Role in Uterine Leiomyomas

Aromatase P450, encoded by the CYP19 gene, is a crucial enzyme involved in estrogen synthesis, with its expression regulated in various tissues through the selective utilization of different promoters. These promoters, corresponding to distinct exons, dictate tissue-specific expression patterns of aromatase mRNA. For instance, gonadal expression predominantly relies on proximal promoters such as PII and I.3, while brain-specific transcription is driven by promoter 1f.

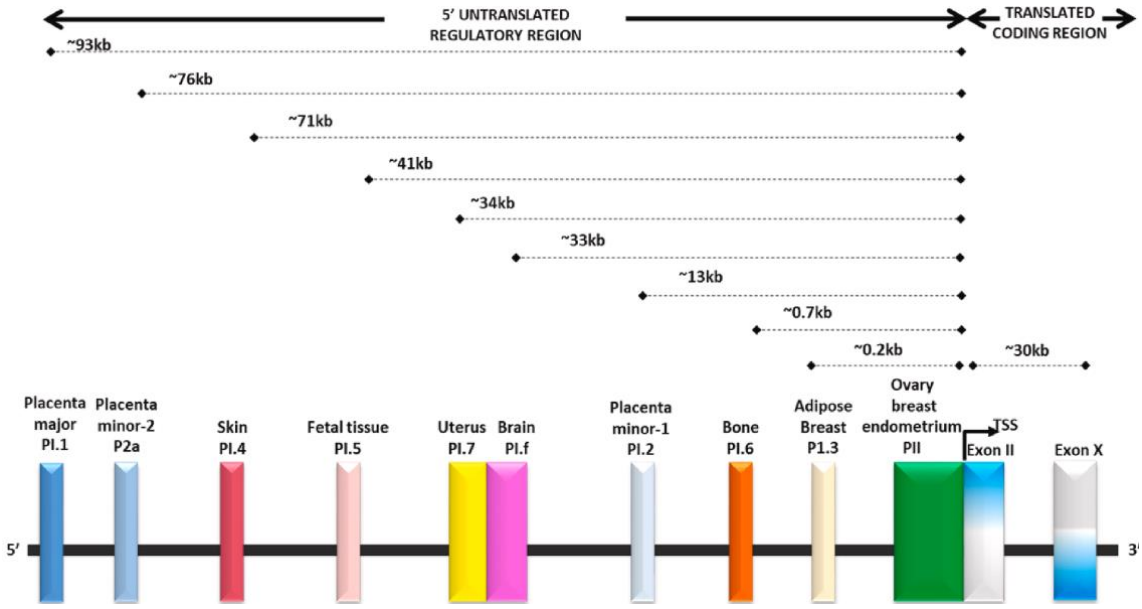

Fig 2: The human aromatase (CYP19A1) gene spans 123 kb, with ten untranslated exons covering 93 kb. Tissue-specific promoters in this region, alongside the transcription start site (TSS) in exon II, regulate gene expression. Eight coding exons follow, constituting 30 kb. Various transcription factors and epigenetic regulators modulate aromatase expression, depicted by arrows indicating upregulation or downregulation (Deborah et al., 2021)

Additionally, adipose tissue and skin utilize promoter I.4, whereas the placenta relies almost exclusively on the distal promoter I.1 (Shozu et al., 2004). This differential promoter usage underscores the complexity of tissue-specific regulation, facilitated by the interaction of cis-

elements with specific transcription factors. Such intricate regulation ensures precise control over estrogen synthesis, vital for various physiological processes (Deborah et al., 2021).

2.8.3.2 Aromatase expression and regulations

The CYP19A1 gene, known for encoding aromatase crucial in estrogen synthesis and cancer progression, exhibits overexpression in cancers, enhancing estrogen levels and tumor growth despite aromatase inhibitor therapy. Recent research implicates Dishevelled (DVL) proteins, integral to Wnt signaling, as novel regulators of CYP19A1 transcription in breast cancer. DVL proteins influence estrogen production by targeting specific CYP19A1 promoters within breast tumors, with loss of DVL-1 and DVL-3 function resulting in distinct alterations in aromatase transcripts and estrogen levels (Deborah et al., 2021). This study illuminates the intricate relationship between Wnt signaling and estrogen synthesis, suggesting potential therapeutic strategies (Castro-Piedras et al., 2018).

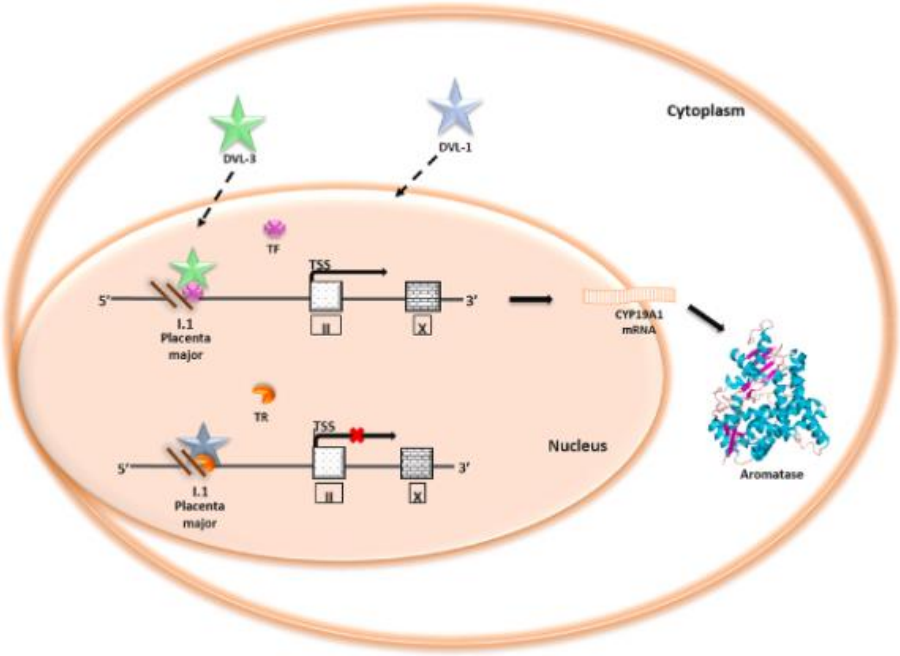

Fig 3: Disheveled proteins, particularly DVL-3, orchestrate the regulation of aromatase transcript at placenta major promoter I.1 by translocating into the nucleus and facilitating the binding of transcription factors. This interaction promotes the initiation of transcription at the specific promoter site, driving the synthesis of CYP19A1 mRNA and subsequent translation into aromatase protein. Conversely, DVL-1 engages with a transcription repressor, leading to the inhibition of aromatase transcription (Deborah et al., 2021)

.

2.9 Wnt Signalling in Cell Differentiation and Proliferation

The Wnt/β-catenin pathway regulates critical transcriptional factors like c-MYC and cyclin-D1, influencing cell proliferation and differentiation. Its dysregulation, often observed in cancer, is associated with aberrant activity in these genes (Rennoll, S., & Yochum, G., 2015). Moreover, this pathway interacts with the PI3K/Akt/mTOR pathway, crucial in cell proliferation. Inhibition of Wnt/β-catenin signaling reduces proliferation, as seen in human embryonic stem cells and uterine leiomyomas. Studies demonstrate that targeting β-catenin and TCF4 inhibits leiomyoma growth in mice, highlighting the pathway's role in leiomyoma cell proliferation (El Sabeh et al., 2021).

2.10 WNT Signaling Pathway

2.10.1 Signaling by WNT

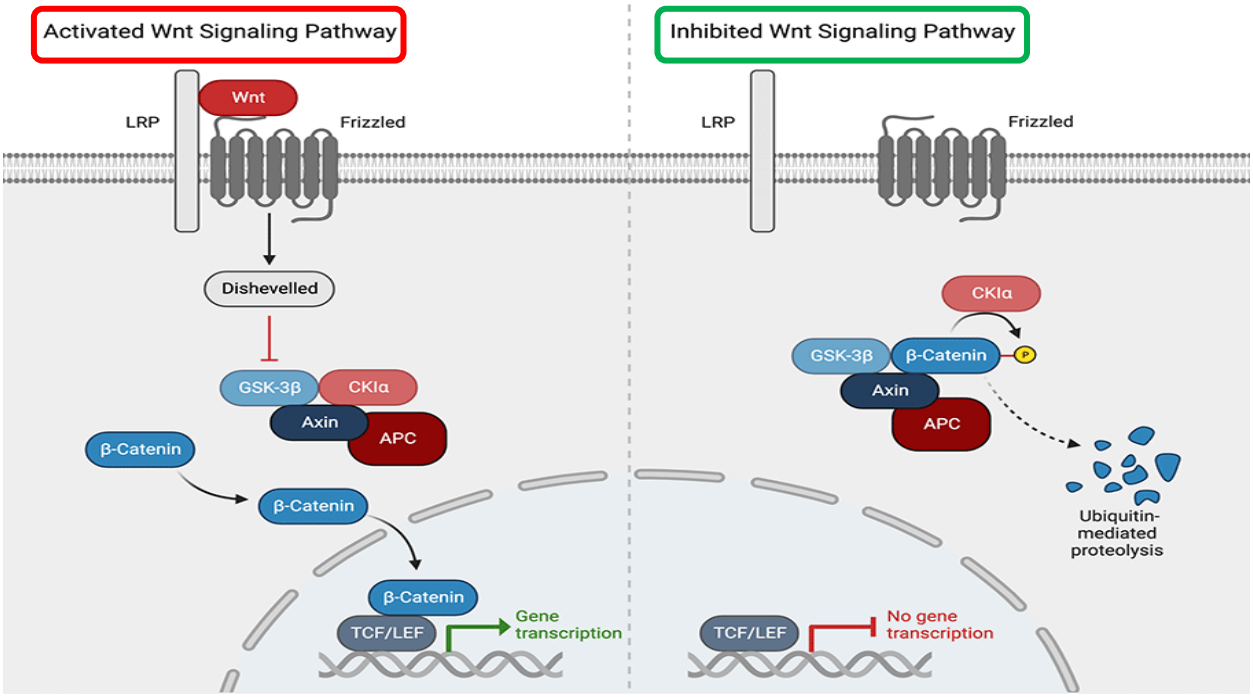

Fig 4: Signaling cascade of Wnt/beta catenin signaling pathway. On the left, Wnt binding to the receptor complex of Frizzled and LRP activates the pathway, leading to β-catenin stabilization and transcriptional activation. On the right, in the absence of Wnt, β-catenin is phosphorylated and targeted for degradation, thus inhibiting the pathway (Zhang & Wang., 2020).

WNT signaling pathways, pivotal in metazoan development and adult processes, govern cell proliferation, fate determination, polarity, and stem cell maintenance (Saito-Diaz et al., 2013; MacDonald et al., 2009). Named after WNT ligands, a diverse family of secreted glycoproteins, these pathways involve at least 19 members with unique expression patterns (Willert and

Nusse, 2012). Upon binding to Frizzled (FZD) receptors and LRP5/6 co-receptors, WNT ligands activate various downstream cascades.

In the canonical pathway, WNT-FZD-LRP engagement stabilizes cytosolic beta-catenin, promoting its translocation to the nucleus where it cooperates with LEF/TCF for transcriptional regulation. Conversely, in the absence of WNT ligand, cytosolic beta-catenin is phosphorylated by a degradation complex comprising GSK3, CK1, Axin, and APC. This phosphorylation marks beta-catenin for ubiquitination and subsequent degradation by the 26S proteasome (Saito-Diaz et al., 2013; Kimmelman and Xu, 2006).

Additionally, WNT signaling orchestrates cellular processes via beta-catenin-independent pathways, such as the non-canonical pathways mediated by Frizzled receptors or tyrosine kinase receptors. These pathways regulate cell migration and polarity, with the planar cell polarity (PCP) pathway governing tissue orientation and development across species (Veeman et al., 2003; James et al., 2009; Seifert and Mlodzik, 2007; Simons and Mlodzik, 2008). Although traditionally considered distinct, evidence suggests interdependence among these pathways, with responses varying based on cellular context and developmental stage (Lai et al., 2009; Schlessinger et al., 2009; Kuhl et al., 2000; Kohn and Moon, 2005; Rao et al., 2010; Minami et al., 2010; van Amerongen and Nusse, 2009).

2.10.1.1 WNT Ligand Biogenesis and Trafficking

WNT proteins, comprising 19 types in humans, are secreted morphogens crucial for various signaling pathways, including the canonical (beta-catenin) and non-canonical pathways like PCP, intracellular calcium regulation, and JNK kinase activation. These ~40kDa proteins are characterized by 23 conserved cysteine residues and are glycosylated and lipid-modified, particularly through PORCN-dependent palmitoylation, essential for their secretion and function (Saito-Diaz et al., 2012; Willert and Nusse, 2012; Janda et al., 2012). Their secretion involves several dedicated factors, such as the Wntless (WLS) sorting receptor, and the SNX3-containing retromer for recycling WLS back to the Golgi (Banziger et al., 2006; Bartscherer et al., 2006; Goodman et al., 2006; Herr et al., 2012; Johannes and Wunder, 2011). WNT proteins interact with extracellular matrix components like HSPGs and may be regulated by proteins such as WIFs and SFRPs. Their diffusion is facilitated by packing into multimers, exosomes, or lipoprotein particles (Gross et al., 2012; Luga et al., 2012; Korkut et al., 2009; Willert and Nusse, 2012).

2.10.1.2 TCF Dependent Signaling in Response to WNT

The WNT signaling pathway involves 19 WNT ligands and 10 Frizzled (FZD) receptors, with interactions varying by development and tissue type, leading to either canonical or noncanonical signaling. In canonical signaling, WNT ligand binding to FZD and LRP receptors deactivates the destruction complex, stabilizes and translocates beta-catenin to the nucleus, and activates TCF/LEF-dependent transcription. This pathway regulates cell fate, proliferation, stem cell renewal, and can contribute to cancer development (MacDonald et al., 2009; Saito-Diaz et al., 2013; Kim et al., 2013).

2.10.1.3 WNT binds to FZD and LRP5/6

The initiation of canonical WNT signaling involves WNT ligands binding to the Frizzled (FZD) receptors, with LRP5/6 acting as co-receptors, although their interaction in vivo is not fully established (Saito-Diaz et al., 2013; He et al., 2004). LRP5/6 can bind directly to certain WNT proteins, but evidence is inconsistent (Tamai et al., 2000; Semenov et al., 2001; Cong et al., 2004; Wu and Nusse, 2002; Mao et al., 2001). Recent crystal structures show in vitro binding of WNTs to LRP6 and FZD8, yet the nature of WNT-receptor interactions in vivo remains unclear (Ahn et al., 2011; Janda et al., 2012; Chu et al., 2013; He et al., 2004; Saito-Diaz et al., 2013).

2.10.1.4 WNT mediated activation of DVL

The three human Dishevelled (DVL) proteins play crucial and overlapping roles in WNT signaling, regulated by phosphorylation. DVL is likely phosphorylated even without WNT stimulation and further modified upon ligand binding by kinases such as CSNK1E, CSNK2, and PAR1 (Willert et al., 1997; Sun et al., 2001; Cong et al., 2004; Ossipova et al., 2005). Upon pathway activation, phosphorylated DVL translocates to the plasma membrane via the DVL PDZ domain and FZD KTxxxW motif interaction, where it oligomerizes and recruits AXIN with assistance from LRP (Wong et al., 2003; Umbhauer et al., 2000; Kikuchi et al., 2011; Schwarz-Romond et al., 2007; Mao et al., 2001). Additionally, DVL promotes the formation of phosphatidylinositol 4,5-bisphosphate by interacting with phosphatidylinositol-4-kinase type II and phophatidylinositol-4-phosphate 5-kinase type I, essential for LRP6 clustering, phosphorylation, and AXIN recruitment (Pan et al., 2008; Qin et al., 2009).

2.10.1.5 FZD recruits DVL to the receptor complex

Dishevelled (DVL) is recruited to the plasma membrane via a direct interaction between its PDZ domain and a conserved motif on Frizzled (FZD) located after the seventh transmembrane region. This recruitment initiates the subsequent recruitment of AXIN and GSK3β to the receptor complex (Fujii et al., 2007; Wong et al., 2003; Zeng et al., 2008; Tauriello et al., 2012).

2.10.1.6 Disassembly of the destruction complex and recruitment of AXIN to the membrane

Upon WNT ligand stimulation, AXIN and GSK3beta are recruited to the plasma membrane via interaction with DVL, enhancing AXIN membrane recruitment through DVL polymerization and GSK3beta/CSNK1-mediated phosphorylation of LRP5/6 (Tamai et al., 2004; Mao et al., 2001; He et al., 2004; Cong et al., 2004; Zeng et al., 2005; Bilic et al., 2007). In some systems like Xenopus oocytes, AXIN's limited concentration makes it a rate-limiting factor for destruction complex assembly (Lee et al., 2003; Benchabane et al., 2008; Tan et al., 2012; MacDonald et al., 2009). WNT signaling reduces AXIN in the destruction complex, increasing free beta-catenin levels (Kikuchi, 1999; Lee et al., 2003). AXIN's association with the destruction complex is regulated by its phosphorylation state, with GSK3beta phosphorylation stabilizing and PP1/PP2A dephosphorylation destabilizing the complex (Luo et al., 2007; Willert et al., 1999; Jho et al., 1999). Additionally, free AXIN is degraded by the 26S proteasome via tankyrase 1 and 2 (Huang et al., 2009).

2.10.1.7 Beta-catenin translocate to the nucleus

The mechanisms controlling beta-catenin localization, despite being crucial for WNT pathway activation, are not fully understood. Beta-catenin, which lacks both NLS and NES, balances between nuclear and cytoplasmic retention through complex interactions. Unlike typical nuclear import, beta-catenin's entry is independent of importins and RanGTPase, potentially interacting directly with the nuclear pore complex due to structural similarities with importin-beta. It may also enter the nucleus by binding with proteins like FOXM1 or BCL9. In the nucleus, beta-catenin is anchored by interactions with TCF, BCL9, and Pygopus. Components of the destruction complex, such as APC and AXIN, also influence its localization. Recent studies suggest Rac1 GTPase and JNK2 are involved in nuclear localization of beta-catenin upon WNT activation, though the precise mechanism remains unclear (MacDonald et al., 2009; Saito-Diaz et al., 2013; Fagotto et al., 1998; Yokoya et al., 1999; Kutay et al., 1997; Malik et

al., 1997; Zhang et al., 2011; Townsley et al., 2004; Tolwinski and Wieschaus, 2001; Krieghoff et al., 2006; Henderson and Fagotto, 2002; Cong and Varmus, 2004; Wu et al., 2008).

2.10.1.8 Formation of the beta-catenin: TCF trans-activating complex

Beta-catenin is crucial for WNT target gene activation, where it interacts with TCF/LEF transcription factors in the nucleus. In the absence of WNT signaling, TCF/LEF proteins recruit Groucho/TLE repressors to inhibit transcription. Upon WNT stimulation, beta-catenin displaces these repressors, enabling transcriptional activation by recruiting various co-activators. Beta-catenin's structure, featuring 12 ARM repeats and N- and C-terminal extensions, facilitates these interactions. Specifically, ARM domains 3-9 bind TCF/LEF, the N-terminal domains 1-4 recruit BCL9, and the C-terminal region interacts with multiple transcriptional activators involved in chromatin remodeling and initiation (Brantjes et al., 2002; Chen and Courey, 2000; Graham et al., 2000; Poy et al., 2001; Xing et al., 2008; Mosimann et al., 2009; Valenta et al., 2012; Willert and Jones, 2006). These interactions likely occur in a sequential manner, ensuring dynamic regulation of gene expression.

2.11 Aberration of WNT Signaling

The Wnt/β-catenin signaling pathway, essential for functions such as cell proliferation, differentiation, and tissue homeostasis, is implicated in the development of both solid and hematological tumors when dysregulated. This pathway's malfunction is strongly associated with cancer initiation and progression, leading to the development of specific inhibitors, antagonists, and agonists for therapeutic intervention in solid tumors (Zhang and Wang., 2020).

2.12 Inhibitors targeting WNT ligand/receptor interface

2.12.1 Porcupine (PORCN) as a target

Porcupine (PORCN), part of the membrane-bound O-acyltransferase (MBOAT) family, is essential for the secretion of Wnt ligands by facilitating their palmitoylation in the endoplasmic reticulum. Inhibitors targeting PORCN can prevent this modification, thereby blocking Wnt secretion. This mechanism has been shown to be effective in treating various cancers. WNT974 (LGK974) is an orally available small molecule inhibitor that reduces epithelial ovarian cancer (EOC) cell viability in vitro and inhibits tumor growth in vivo.

2.12.2 LRP5/6 as a target

In the Wnt/β-catenin signaling pathway, the co-receptor LRP5/6, upon phosphorylation, enhances pathway activation. The formation of the Wnt-FZD-LRP5/6-DVL complex facilitates AXIN interaction, which in turn inhibits β-catenin degradation.

2.12.3 DVL as a target

DVL plays a crucial role in Wnt signal transduction by recruiting components of the β-catenin destruction complex to the cell membrane. It binds to the cytoplasmic carboxyl terminal end of FZD proteins via its PDZ domain. Agents such as NSC668036, FJ9, and 3289–8625 hinder the DVL-PDZ interaction, thereby inhibiting the signal transduction pathway. FJ9, with its non-electrophilic indole-2-carbinol-based chemical scaffold, disrupts the interaction between FZD and the PDZ domain of DVL. NSC668036 and 3289–8625 have been shown to down-regulate Wnt/β-catenin signaling and inhibit tumor cell growth in lung, colorectal, and cervical cancer cell lines in vitro, as well as in lung cancer xenografts (Zhang and Wang., 2020).

2.12.4 Inhibitors targeting the beta-catenin-destruction complex

2.12.4.1 Beta-catenin/TCF interface as a target

The Wnt/β-catenin signaling pathway is pivotal in development, tissue maintenance, and cancer. β-catenin, existing in various cellular locations, undergoes degradation unless stabilized by Wnt ligands. Nuclear β-catenin accumulation drives tumorigenesis by enhancing pro-growth gene expression. In uterine fibroids (UFs), elevated nuclear β-catenin correlates with increased proliferation and expression of growth-promoting genes like cyclin D1 and c-Myc. Inhibiting β-catenin in UFs reduces cell growth, while its activation promotes it (Ali et al., 2020).

2.12.4.2 DIX domain of AXIN and DVL as a target

The DIX domain within Dvl and Axin proteins facilitates their interaction, crucial for Wnt signaling pathway activation (Choi et al., 2010; Fiedler et al., 2011). Targeting this domain in both proteins could potentially inhibit aberrant downstream signaling (Gammons et al., 2016).

2.12.4.3 PP2A as a target

Cell division, a complex phenomenon intricately governed by various proteins, notably kinases and phosphatases, has historically emphasized the role of kinases over phosphatases. However, recent research underscores the critical involvement of phosphatases, particularly Protein

Phosphatase 2A (PP2A), in orchestrating precise control over the cell cycle, including tumor suppression mechanisms (Wlodarchak & Xing, 2016). Within the Wnt signaling pathway, PP2A assumes a multifaceted role in modulating β-catenin activity, a central component of Wnt signaling. It operates through distinct isoforms, exhibiting both positive and negative regulatory effects on β-catenin. While PP2A-Bα holoenzyme enhances Wnt signaling by directly dephosphorylating β-catenin, thereby stabilizing it, PP2A B′α holoenzyme antagonizes this process by associating with the destruction complex, leading to reduced β-catenin levels. Furthermore, PP2A influences Wnt signaling indirectly by targeting key regulators like GSK3β, wherein it promotes β-catenin degradation. These insights position PP2A as a promising therapeutic target for diseases linked to dysregulated Wnt signaling, such as cancer, offering avenues for precise intervention and drug discovery (Wlodarchak & Xing, 2016).

2.12.4.4 DEP domain of DVL as target

DEP dimerization is a pivotal process for the formation of functional signalosomes, a crucial step in Wnt signal transduction. Through domain swapping, a DEP monomer extends its N-terminal α-helix to interact with another DEP monomer, as elucidated by crystallography (Gammons et al., 2016).

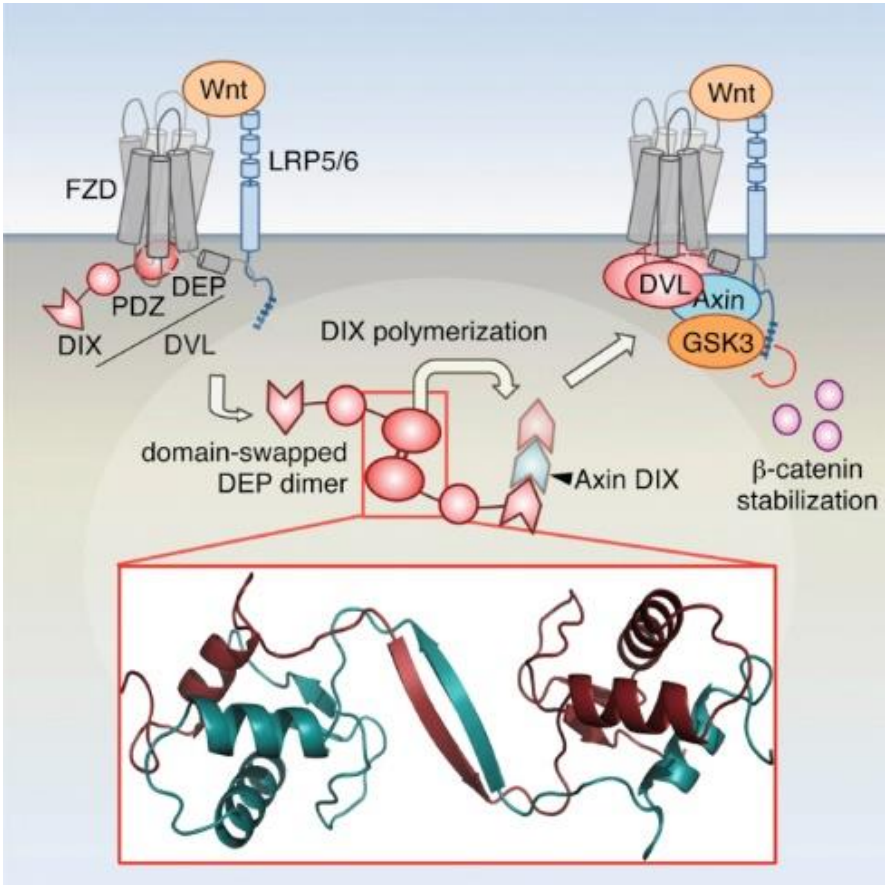

Fig 5: DEP-DEP homodomer formation activating Wnt Signalosome assembly (Gammons et al., 2016).

This conformational switch in Dishevelled, driven by DEP domain swapping, is indispensable for assembling functional signalosomes and transmitting Wnt signals to the nucleus. DEP-mediated dimerization of Dishevelled promotes tetramerization, which impedes its binding to Frizzled receptors. Moreover, it enhances the local concentration of associated DIX domains, facilitating their avid interaction with Axin DIX and initiating the stabilization of β-catenin through hetero-polymerization, a critical event in Wnt signaling pathways (Gammons et al., 2016).

In summary, the intricate Wnt signaling pathway presents promising opportunities for therapeutic intervention in cancer and other diseases. Targeting key components such as Porcupine, LRP5/6, DVL, and the β-catenin destruction complex holds potential for precise treatments (Author, Year). Continued research and development of inhibitors underscore the potential for tailored precision medicine approaches, promising a revolution in cancer treatment.

2.13 Reference protein for ligand library preparation

2.13.1 S-Adenosyl L-methionine

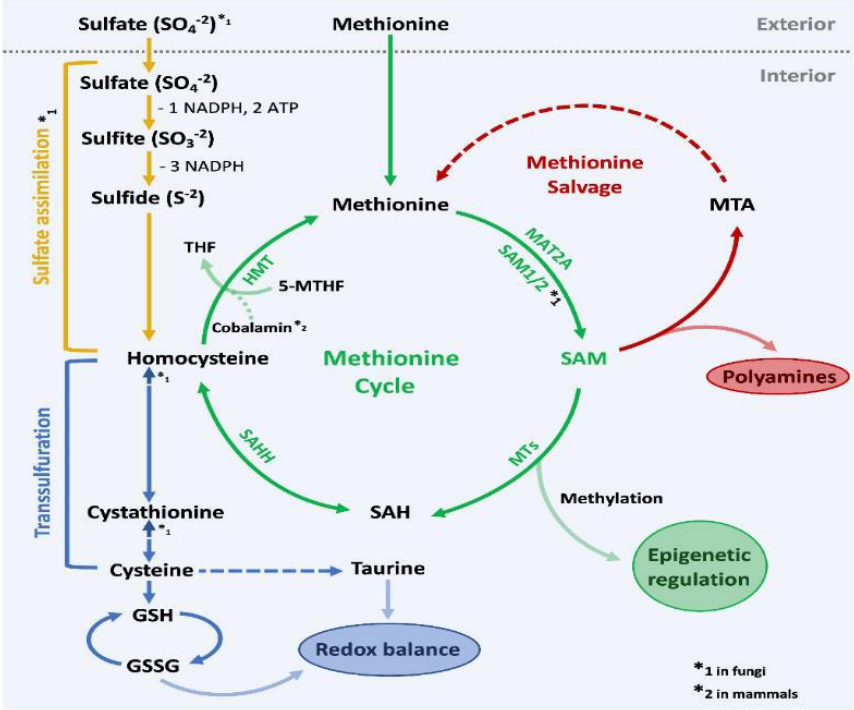

Figure 6: Overview of the methionine cycle and other tightly coupled metabolic pathways (Lauinger and Kaiser,2021).

S-Adenosyl-L-methionine (AdoMet or SAM) is a significant sulfonium molecule in biological systems, serving as a vital cofactor for methyl group transfer reactions catalyzed by SAM-

dependent methyltransferases (MTases). These reactions play crucial roles in various biological

processes, including epigenetic regulation, protein modulation, metabolite synthesis, and signaling. Additionally, SAM is involved in transsulfuration pathways, linking it to cysteine biosynthesis, polyamine formation, and radical-mediated biochemical transformations (Zhang & Zheng, 2016; Ouyang et al., 2020).

Understanding the methionine cycle is crucial as S-adenosylmethionine (SAM) plays a pivotal role, with enzymes like methionine adenosyl transferase (MAT2A) and SAM synthetase (SAM1/2) involved. Methyltransferases (MTs), S-Adenosyl homocysteine hydrolase (SAHH), and Homocysteine methyltransferase (HMT) are also integral to this cycle. Byproducts from the methionine salvage pathway are recycled to regenerate methionine. Homocysteine is converted to cysteine via the transsulphuration pathway, contributing to glutathione (GSH) and taurine synthesis for cellular redox balance. Fungi can synthesize methionine from absorbed sulfate via the energy-intensive sulfur assimilation pathway, requiring 2 ATP and 4 NADPH per methionine molecule (Lauinger, L. and Kaiser, P., 2021).

2.13.2 Methionine Adenosyltransferase/ *S*-Adenosyl *L*-methionine Synthetase

Methionine adenosyltransferase (MAT) is a ubiquitous enzyme found across various organisms, from bacteria to mammals, responsible for catalyzing the formation of S-adenosylmethionine (SAM) using L-methionine and ATP (Markham and Pajares, 2009). Mammals possess multiple isoforms of MAT enzymes, including MAT1A, MAT2A, and MAT2B, encoded by different genes such as mat1a, mat2a, and mat2b. MAT1A, found in the adult liver, exists in both tetrameric and dimeric forms and plays a crucial role in transmethylation reactions. In contrast, MAT2A, predominantly expressed in fetal liver and non-hepatic tissues, forms a dimer and functions differently from MAT1A. MAT2B interacts with MAT2A and modulates its catalytic activity by altering the affinity for substrates like L-methionine and SAM (LeGros et al., 2000; Xia et al., 2010).

Mutations in the mat1a gene have been associated with isolated persistent hypermethioninemia and hepatic MAT deficiency, contributing to liver diseases such as cirrhosis and hepatocellular carcinoma (HCC) (Gaull et al., 1974; Martínez-Chantar et al., 2003). In HCC, there is a shift in MAT protein expression from MAT1A to MAT2A/MAT2B, promoting rapid cell growth and cancer progression (Martínez-Chantar et al., 2003; Wang et al., 2008). SAM biosynthesis by hepatic MAT1A and extrahepatic MAT2A is crucial for maintaining hepatic health, and

deficiencies in SAM production are associated with increased inflammation (Lu et al., 2002; Avila et al., 2005). Additionally, low SAM levels have been observed in Alzheimer's disease, prompting research into SAM-fortified prevention strategies (Scarpa et al., 2006).

2.14 Human Cytochrome P450 enzymes and its sub-family

Cytochrome P450 enzymes, notably CYP2C9, CYP2C19, CYP2D6, and CYP3A4, play crucial roles in metabolizing various substances, including drugs and environmental chemicals. The CYP3A subfamily, particularly CYP3A4, located on chromosome 7q21–q22, is highly significant, with CYP3A4 being predominant in the small intestine and adult liver. The gene cluster contains four functional genes with 13 exons each, interspersed with pseudogenes. Single nucleotide polymorphisms (SNPs) affecting CYP3A4 and CYP3A5 are distributed across the gene structure, potentially influencing metabolic activity (Parikh et al., 1997; Finta and Zaphiropoulos, 2000; Perrotti & Neviani, 2008).

2.14.1 Relevance of CYP3A4 to drug discovery

In contemporary medical practice, assessing a drug candidate's metabolic profile and potential interactions with existing medications is paramount. Negative drug-drug interactions (DDIs) can result in increased systemic exposure to a drug, leading to toxicity and slow elimination. For instance, the interaction between terfenadine and CYP3A4 inhibitors led to terfenadine's withdrawal from the market due to cardiotoxicity risk (Decherchi & Cavalli, 2020). Similarly, the concurrent use of temsirolimus and dexamethasone in patients with advanced renal cell carcinoma resulted in reduced temsirolimus plasma levels, illustrating the impact of DDIs on drug clearance and efficacy (Staeheler et al., 2010).

2.15 Phase I Drug Metabolizing Enzymes

Drug metabolizing enzymes, also known as mixed function oxidases or monooxygenases, encompass various components such as cytochrome P450, cytochrome b5, NADPH-cytochrome P450 reductase, and others (Pfeffer, 1975). Among these, cytochrome P450 enzymes (CYPs or P450s) stand out as pivotal players in the phase I metabolism of drugs and toxins in humans (Zollner et al., 2010).

CYP1A1, a prominent member of the cytochrome P450 family, has been extensively studied for its role in activating carcinogenic compounds while also participating in the detoxification of environmental carcinogens and metabolic activation of dietary cancer-preventative compounds. Similarly, CYP1A2, another cytochrome P450 enzyme, is vital for drug

metabolism and lipid production, with its expression influenced by certain polycyclic aromatic hydrocarbons (Zollner et al., 2010).

Another crucial enzyme, CYP2D6, plays a significant role in metabolizing approximately 20% of commonly prescribed drugs across various medical specialties, despite exhibiting high levels of polymorphism (Zollner et al., 2010). Similarly, CYP2E1 metabolizes procarcinogens, solvents, medicinal drugs, and endogenous compounds, potentially generating harmful metabolites and oxidative stress (Zollner et al., 2010).

CYP1B1, a member of the CYP superfamily, not only metabolizes xenobiotics but also regulates endogenous metabolic pathways, aiding in the homeostasis of substances like steroid hormones and vitamins (Zollner et al., 2010).

Additionally, CYP2C9, responsible for metabolizing pharmaceuticals and endogenous substances, exhibits high polymorphism, affecting its metabolic efficiency (Wikipedia). In summary, these enzymes collectively play pivotal roles in drug metabolism, toxin detoxification, and the maintenance of metabolic homeostasis.

2.16 Virtual Screening or computational review

2.16.1 Virtual Screening

High-Throughput Screening (HTS) remains a pivotal method for discovering biologically active compounds, yet its widespread application in drug discovery is hampered by high operational costs (Sliwoski et al., 2013). In contrast, recent advancements have propelled virtual screening into the forefront of drug discovery, enabling the rapid selection of potential candidates from vast chemical libraries with reduced time and expense (Song et al., 2009; Macalino et al., 2015). Virtual screening employs computational techniques to identify compounds that best interact with target proteins, offering a cost-effective and efficient alternative to traditional HTS methods (Pinzi and Rasteli, 2019).

2.16.1.1 Virtual Screening Types

Virtual screening has become increasingly valuable in drug discovery, particularly for lead identification, lead optimization, and scaffold hopping, due to its speed and cost-effectiveness compared to high-throughput screening (John et al., 2010). There are two main computational techniques for virtual screening: ligand-based and structure-based methods. This study focuses on structure-based virtual screening, utilizing the structural information of the coronavirus

main protease for drug discovery. Ligand-based virtual screening relies on the similarity of physio-chemical structures among active ligands to enhance drug-like properties, while structure-based methods, or ligand docking, use 3D protein structures to analyze binding poses and affinities (Hamza et al., 2012).

2.16.1.1.1 Ligand-Based Virtual Screening (LBVS)

LBVS relies on known active ligands to identify and optimize leads, making it suitable when the 3D structure of the target protein is unavailable (Hamza et al., 2012). This method involves finding new ligands by assessing their similarity to established active compounds, provided there is at least one known active compound against the target (Tresadern et al., 2009). Key factors for LBVS include effective similarity measures and reliable scoring functions (Hamza et al., 2010).

2.16.1.1.2 Structure-Based Virtual Screening (SBVS)

SBVS, or target-based virtual screening, predicts the best fit between ligands and a molecular target using the 3D structure of the target protein (Liu et al., 2018). Molecular docking, a prominent SBVS technique, benefits from low computational costs and advances in computational power since the 1990s (Meng et al., 2011; Kuntz et al., 1982). Despite challenges in parameterizing ligand-receptor interactions and predicting accurate binding poses (Lionta et al., 2014), SBVS is advantageous for saving time and resources in drug discovery (Maia et al., 2020). Recent studies have effectively employed SBVS in drug research (Carpenter et al., 2018; Dutkiewicz and Mikstacka, 2018; Nunes et al., 2019).

2.16.1.2 Considerations in Structure-Based Virtual Screening

In structure-based virtual screening (SBVS), obtaining the 3D structure of the target protein is essential. This can be sourced from experimental data (e.g., X-ray crystallography, NMR, neutron scattering), homology modeling, or molecular dynamics simulations. Critical considerations include the receptor's druggability, choice of binding site, selection of the most relevant protein structure, receptor flexibility, appropriate protonation states, and the role of water molecules in the binding site (Reddy et al., 2007). Accurate prediction of ligand binding sites and careful preparation of the compound library—ensuring correct stereochemistry, tautomeric, and protonation states—are also crucial. Once the ligand library and receptor are prepared, compounds are docked into the target binding site using docking programs, which predict the ligand-protein complex structure and calculate the binding free energy using scoring

functions. This process ranks potential compounds for further experimental validation (Koppen, 2009).

2.16.1.2.1 Protein preparation

Proper starting structures for both protein and ligand are crucial in Structure-Based Virtual Screening (SBVS). Protein Data Bank (PDB) files often contain heavy atoms, water molecules, cofactors, activators, ligands, metal ions, and multiple protein subunits, but may lack accurate bond orders, topologies, or atomic charges. Issues like misarranged terminal amides and asparagine residues, unassigned ionization and tautomeric states, missing residue side chains or loops, and potential steric clashes are common due to X-ray structure limitations (Lionta et al., 2014). To address these, several protein preparation tools and methods have been developed. Software such as PROPKA (Li et al., 2005), H++ (Anandakrishnan et al., 2012), and SPORES (ten Brink and Exner, 2010) calculate protein protonation states, while PDB2PQR (Dolinsky et al., 2007) optimizes hydrogen bonding networks. Further steps include assigning partial charges, capping residues, treating metals, filling missing loops and side chains, and minimizing structure to reduce steric clashes (Young et al., 2007). Additionally, deciding whether to retain or remove water molecules from the binding site is critical, with several methods available to address this (Michel et al., 2009). Employing comprehensive protein preparation schemes significantly enhances docking performance over using minimally prepared PDB structures (Sastry et al., 2013).

2.16.1.2.2 Binding site Identification

Accurate binding site prediction is crucial for successful structure-based virtual screening (SBVS). Several approaches are employed for this task. Static methods, such as FTMap (Ngan et al., 2012) and Fpocket (Le Guilloux et al., 2009), use computational solvent mapping with chemical probes to identify binding hotspots on 3D protein structures derived from X-ray crystallography or molecular dynamics. Dynamic methods involve the evolution of probes and proteins over time, using interaction free energies to locate binding sites, exemplified by MDMix (Seco et al., 2009). Another technique employs water molecules as probes to predict binding sites, as seen in JAWS (Michel et al., 2009).

2.16.1.2.3 Compound Library Preparation

In the realm of structure-based virtual screening (SBVS), the assembly of a diverse compound database is crucial. This entails the selection or synthesis of small drug-like molecules

possessing favorable attributes such as stability, aqueous solubility, appropriate functional groups for interaction with biological targets, and a lack of toxicity. The renowned "Lipinski Rule of Five" serves as a benchmark for drug-likeness evaluation (Lipinski et al., 2001).

Table 1: Criteria for Drug-Like Properties: Lipinski's Rule of Five Parameters

Parameter	Lipinski Rule of Five
Molecular Weight	< 500
Lipophilicity (logP)	< 5
Hydrogen Bond Donors	< 5
Hydrogen Bond Acceptors	< 10

The definition of drug-likeness encompasses various parameters, including molecular weight, lipophilicity, and hydrogen bond interactions, as outlined by the Lipinski Rule of Five. However, extensions such as Pfizer's Rule of 3/75 and Jorgensen Rule-of-Three offer refined criteria, emphasizing factors like ClogP, TPSA, and cellular permeability to enhance predictions of in vivo safety and efficacy.

Table 2: Criteria for Drug-Like Properties: Summary of Physicochemical and Pharmacokinetic Guidelines

Property	**Range or Criterion**	**Rule/Rules**
LogP	-0.4 to +5.6	Veber et al. (2002)
Molar Refractivity	40 to 130	Veber et al. (2002)
Molecular Weight	180 to 500	Veber et al. (2002)
Number of Atoms	20 to 70	Veber et al. (2002)
Polar Surface Area	< 140 Å^2	Veber et al. (2002)
Rotatable Bonds	< 10	Veber et al. (2002)
ClogP	< 3	Pfizer's Rule of 3/75 (Hughes et al., 2008)
TPSA	> 75 Å^2	Pfizer's Rule of 3/75 (Hughes et al., 2008)

Aqueous Solubility (LogS)	> -5.7	Jorgensen Rule-of-Three (Kerns and Di, 2008)
Caco-2 Cell Permeability	Faster than 22 nm/s	Jorgensen Rule-of-Three (Kerns and Di, 2008)
Number of Primary Metabolites	< 7	Jorgensen Rule-of-Three (Kerns and Di, 2008)

To effectively assess the drug-likeness of small molecules, it is crucial to adhere to established guidelines that consider various physicochemical and pharmacokinetic properties. These guidelines establish thresholds or ranges indicative of desirable characteristics for drug development, including favorable pharmacokinetics, bioavailability, and safety profiles (Athanasiadis et al., 2012). During compound selection for virtual screening, prioritizing lead-like properties, excluding known toxicophores, and avoiding blind docking of large compound libraries like PubChem and ChemSpider are essential steps. Utilizing online tools such as Chembioserver streamlines compound filtration based on ADMET properties, facilitating preparation for virtual screening (Athanasiadis et al., 2012). Additionally, ensuring realistic 3D representations with correct bond lengths, angles, and physicochemical properties is paramount. Ligand preparation software such as Autodock Tools plays a pivotal role in guaranteeing proper compound setup for docking simulations (Morris et al., 2009).

2.16.1.2.4 Library Design

Developing a tailored library, rather than relying on publicly available resources, could enhance the efficacy of Structure-Based Virtual Screening (SBVS) procedures (Lavecchia and Di Giovanni, 2013). Tools like CLEVER facilitate chemical library manipulation, combinatorial enumeration, format conversion, and compound analysis, aiding in the design process by filtering compounds based on drug-likeness, lead-likeness, and fragment-likeness (Song et al., 2008). Similarly, e-LEA3D enables scaffold-based library design using user-provided scaffolds and reactants, potentially sourced from chemical vendors (Douguet, 2010).

2.16.1.2.5 Docking and scoring functions

The current landscape of docking programs includes AutoDock, Dock, FlexX, and Glide, among others. These programs utilize various methods, such as systematic and stochastic searches, as well as molecular dynamics simulations, to explore ligand conformational space (Morris et al., 2009; Ewing et al., 2001; Rarey et al., 1996; Friesner et al., 2004; Cheng et al.,

2012). Scoring functions, such as ChemScore and Fresno, estimate the free energy of ligand-target association based on chemical interactions and solvation effects (Cheng et al., 2012; Lionta et al., 2014). Development of accurate scoring functions, including considerations for protein flexibility, is crucial for the effectiveness of structure-based virtual screening (SBVS) (Spitzer et al., 2012).

2.16.1.2.6 Post Processing

In the realm of structure-based virtual screening (SBVS), post-processing poses challenges due to issues like unrealistic conformations and imperfect scoring functions (Waszkowycz, 2008). Correct compound selection necessitates meticulous visual inspection (Athanasiadis et al., 2012). Directional methods like Molecular Interaction Energy Components (MIECs) aid in accurate affinity prediction (Ding et al., 2013). Free Energy of Binding (FEB) rescoring and Vdw filtering techniques contribute to efficient lead identification (Malmstrom et al., 2012; Athanasiadis et al., 2012). Additionally, hierarchical clustering assists in identifying compounds with similar properties (Lionta et al., 2014).

2.16.1.2.7 Advancements in SBVS

The limited information provided by a single protein conformation, influenced by crystallization conditions, hampers the efficiency of Structure-Based Virtual Screening (SBVS) as it may overlook conformational changes post-ligand binding. Incorporating receptor flexibility into docking programs through ensemble docking or Consensus induced fit docking (cFID) addresses this issue. While ensemble docking considers multiple rigid receptor conformations, cFID allows the protein binding site to adapt to different ligands, enhancing pose prediction accuracy. However, challenges include increased computational demand and potential inaccuracies in scoring functions (Korb et al., 2012; Craig et al., 2010; Osguthorpe et al., 2012; Houston and Walkinshaw, 2013; Kadid et al., 2013).

2.17 Review on software used in this study

2.17.1 Auto Dock

The software suite AutoDock, developed at the Scripps Research Institute in the 1990s, is a powerful tool for predicting ligand-receptor interactions in molecular docking studies (Morris et al., 2009). It offers fast and accurate predictions, making it widely utilized in research and education (Helgren & Hagen, 2017). AutoDock's graphical user interface (ADT) enhances user interaction by facilitating molecular visualization and analysis, particularly beneficial for

educational purposes. Its ability to conduct blind docking, where the binding site is unknown, further extends its applicability (Morris, 2007). AutoDock's utilization of simulated annealing and grid-based energy evaluation techniques enhances the efficiency and accuracy of ligand conformation searches (Goodsell and Olson, 1990; Lybrand, 1995; Rosenfeld et al., 1995).

2.17.2 Osiris datawarrior

Datawarrior, developed by Actelion Pharmaceuticals Ltd., is an open-source data visualization and analysis software with robust chemical intelligence features (Sander et al., 2015). It integrates dynamic graphical views with chemical descriptors, enabling the visualization of compound structures and properties (Sander et al., 2015). Through its support for various molecular similarity calculations and ADME/Tox property filtration, Datawarrior aids in the exploration and optimization of compound libraries (Sander et al., 2015).

2.17.3 PyMol

PyMOL, an open-source molecular graphics tool initially developed by Warren Lyford Delano and later commercialized by Schrödinger Inc., is widely utilized in drug discovery for protein and small molecule visualization (Yuan et al., 2017). Its versatile features include active site determination, molecular editing, and the creation of molecular movies, enhancing its utility in structure-based drug design (Yuan et al., 2017). PyMOL's extensibility through Python plugins further augments its capabilities, enabling customization to specific research needs (Yuan et al., 2017).

2.17.4 ChimeraX

ChimeraX, developed by the Resource for Biocomputing, Visualization, and Informatics (RBVI), is a next-generation molecular visualization program offering significant performance enhancements and new analysis features. With support for virtual reality and medical imaging data, ChimeraX extends beyond atomic-scale visualization to accommodate larger-scale datasets. Its intuitive user interface and app store for user-contributed tools enhance usability and functionality, making it a valuable asset for diverse life science applications.

2.17.5 Discovery Studio Visualizer

Discovery Studio Visualizer by Dassault Systems BIOVIA is a feature-rich molecular modeling application that facilitates the visualization, sharing, and analysis of protein and small molecule data. Its interactive environment supports diverse visualization capabilities, including

stereo graphical options and interactivity between graphical views. With support for sequences, 2D/3D charting, and data tables, Discovery Studio Visualizer offers comprehensive tools for molecular analysis and exploration (Dassault Systemes Biovia Corp.).

2.17.6 PyRx

PyRx, an open-source virtual screening software, aids in screening compound libraries against drug targets in computational drug discovery. Utilizing AutoDock and AutoDock Vina for docking, PyRx offers a user-friendly interface and powerful visualization engine for rational drug design. Its integration of established open-source software and support for chemical spreadsheet-like functionality make it a valuable tool in the drug discovery process.

2.17.7 Gaussian

Gaussian, a renowned computational chemistry software, originated in 1970 under the leadership of John Pople at Carnegie Mellon University, initially known as Gaussian 70. Over the years, it has evolved into Gaussian 03 version 6.0, developed by Gaussian Inc., becoming a staple tool for chemists and scientists worldwide in analyzing computational data (Pople, 2004).

CHAPTER 3

MATERIALS AND METHODOLOGY

3.1 Protein target identification and processing

The protein target chosen for this study is the co-crystal structure of PORCN, PDZ, DEP and DIX domain of DVL and DIX domain of AXIN, set of crucial protein responsible for ligand trafficking of Wnt ligands to the receptor and activation of downstream process of Wnt signaling targeting to intervene the conversion of uterine stem cells into cancer cells. The corresponding PDB file (ID: 7URD, 2KAW, 5LNP and 6JCK) was obtained from the RCSB Protein Data Bank.

Additionally, hMAT1A (PDB ID: 6S5W) and hCYP3A4 (PDB ID:) was taken as a reference protein target in preparing ligand library.

3.1.1 Validation of retrieved 3D structure of protein

The retrieved 3D structure were subjected to Ramachandran plot analysis for structure validation using SAVES online tool.

3.1.2 Protein processing and preparation

For the identification of active site, amino acid within 5Å with of bound native ligand was visualized via PyMol, RCSB database accessing ligand interaction option from the website itself and was later also confirmed via ChimeraX software.

While for predicting the binding site of DEP domain of DVL targeting its homodimerization, and DIX domain of DVL and AXIN, the interacting interface residues was visualized in PyMol, using ‘Polar Contacts’ option from the software itself.

Then the retrieved proteins were processed in PyMol a protein visualization tools where cofactors, water molecules and native ligands were removed and then was exported for further processing. The exported structure were accessed using AutoDock tools (Trott & Olson, 2010), where modifications were made to prepare them for molecular docking. This involved the addition of hydrogen bonds, merging non-polar surface areas, and computing charges using the Gasteiger method. Then the file was converted to pdbqt format for further docking studies within the AutoDock tool.

3.2 Ligand library preparation

Ligand library of natural products were selected for the present study. This ligand library was downloaded from Zinc15 database (www.zinc15.docking.org) from which total of 224405 molecules were retrieved in sdf format.

The retrieved ligand library was then primarily screened for druggability based on Lipinski's rule of five and LogS (Benet *et.al.,* 2016) for better absorption, distribution, metabolism and excretion. Natural products having molecular weight between 200 to 500 Da, cLogP (lipophilicity) -3 to 6, cLogS (water solubility) -4 to -2, hydrogen bond acceptor 0 to 10, hydrogen bond donor 0 to 5 were selected. Furthermore, ligands having the positive value between 0 to 15 for druglikeliness, Vaber's rule (Vaber *et.al.,* 2002) was applied; topological polar surface area 1 to 120 and rotatable bond count 0 to 10 especially for oral bioavailability. In addition, ligands with non-tumorigenic, non-mutagenic, non-irritant and non-reproductive effects were finally screened using OSIRIS data warrior (López-López *et.al.,* 2019).

The ligand pool were then reduced to 35834 ligands, which were then saved in sdf format for further processing. The ligands were then subjected to PyRx interface, for further processing of energy minimization and conversion of file format from sdf to pdbqt for usage in docking.

3.2.1 Energy minimization:

Energy minimization was performed with the universal force field (UFF) using the conjugate gradient algorithm in available in PyRx interface. From which 300 of the ligands failed this step of minimization step and was discarded. So, only 35534 ligands were converted to pdbqt file format using OpenBabel GUI interface in PyRx.

3.2.2 Filtration of ligand library using reference protein:

3.2.2.1 hMAT1A as primary filter:

The hMAT1A filter had been employed to eliminate ligands disrupting cellular processes and harming the liver by substituting the native ligand SAM of hMAT1A. The ligand-free crystal structure of human S-adenosylmethionine synthetase 1 (hMAT1A protein) (RCSB id: 6SW5) was chosen for filtration. Following modification in Pymol, the hMAT1A protein had been prepared by eliminating Chains C and D, retaining only Chains A and B. Any water molecules were also removed.

Prior to docking, the modified protein had been converted to the pdbqt format using Autodock tools. Initial docking was performed using a ligand library, with SAM serving as the reference inhibitor. The hMAT1A filtered ligands, where those with binding energies lower than SAM inhibitor were retained, and those with higher energies were excluded. Furthermore, these filtered ligands underwent additional screening using the protein CYP3A4 to identify lead compounds for potential drug candidate development.

3.2.2.2 hCYP3A4 filter for drug metabolism

Following the initial screening utilizing hMAT1A, the refined ligand library was employed for the preliminary docking procedure with the CYP3A4 protein. Ritonavir (RIT) served as the benchmark inhibitor during the screening process. Subsequently, alongside the hMAT1A filtered ligands, the filtered ligands from CYP3A4 were utilized for the conclusive molecular docking aimed at identifying lead targets subsequent to the virtual screening. Ligands exhibiting binding energies lower than that of the RIT inhibitor were retained, while those with higher energies were excluded.

3.3 Screening of putative drug candidate

3.3.1 Molecular docking

The filtered ligands had been employed in molecular docking through Autodock Vina within the PyRx interface, alongside the inhibitor for our prioritized proteins for binding energy analysis. The docking procedure had been executed with an exhaustiveness value of 32 and a mode count of 32. Following this, all ligands had been arranged based on their binding energies, and those with binding energies greater than the inhibitors had been chosen as hits for further processing and study.

3.3.2 Identification of top hits

For further screening the selected ligands were again docked with the Phase I drug metabolizing enzymes (cytochrome P450s enzymes), for safety purpose as the slected ligands from this filter should not inhibit in filtering of the xenobiotics from the body. All the ligands with the lower binding energies than the inhibitor of each cytochrome P450s enzymes selected in this study were taken into further processing.

We had established stringent parameters for the preference index, which involved considering the number of H-acceptors, H-donors, and rotatable bonds within the pharmacophore. This formula was crafted as follows:

(H-acceptor count + H-donor count + rotatable bond count) multiplied by 5, all divided by 25.

Ligands underwent final screening based on its higher binding energy against the target protein and a higher value of the preference index, alongside lower binding energy against human hepatic and SAM synthetase proteins and cytochrome P450s enzymes, in this way screening of top hits was done.

3.3.3 Final screening of potential lead compound

Screened top hits were then subjected to DFT analysis using Gaussian 03W using B3LYP function and 6-31G basis set as a calculation setup for the calculation of total energy, Dipole moment, and energy gap for understanding the better stable ligand with reactive structure and with preferred dipole moment as a good drug target.

Based on this calculation analysis was further done to screen putative lead molecules.

3.4 Protein-Ligand interaction

3.4.1 Bonding of ligands with amino acids at active sites

After the molecular docking and screening of lead molecules with stringent parameters, the selected molecules were subjected to determine protein-ligand interactions. Macromolecules, in which the ligand bound to the active sites of the protein, had been utilized from the file generated in PyRx after successful docking performance.

The 2D interactions between the target proteins and potential lead were analyses using Biovia Discovery Studio 2020 Client was used. The target protein from the working directory macromolecules created for PyRx, was dragged into the interface of discovery Studio software and then the potential lead molecule was also dragged over the protein structure. Then, the interaction between protein and ligand was analyzed. Under protein ligand interaction, type of bond formed between the interacting residues and ligand was observed based on the bond types. Its category, length etc. which further elucidate the affinity of bonding of ligand to the protein molecule.

3.5 Thermochemical analysis

For the screening of putative lead compound, total energy of the molecule, RMSD, dipole moment, energy gap (HOMO-LUMO gap) were calculated using DFT analysis using Gaussian 03W package. For further analysis of the interaction between the protein or interacting residues with the potential lead, the output from the calculation was view into Gauss view 05 as visualization tool. The potential lead compound were looked further for molecular electrostatic potential graph or surface, indication the role of ligand atoms form electron transport between the molecules.

Beside that frontier HOMOs and LUMOs and gap energy was calculated and visualized for further investigation of electron transport properties.

3.6 Molecular Dynamic Simulation

The pdb files of protein-ligand complexes; of *PORCN in complex with ligand 42151* were taken to study binding mechanism, flexibility and stability of the complexes. CHARMM-GUI (Lee *et.al.,* 2016) was used to generate new psf, protein structure file that contains all of the molecule-specific information needed to apply a particular force field and pdb files and both the complexes were solvated in TIP3P water model in a cubical box of equal dimensions 121 × 121 × 121 Å3 and electrically neutralized by adding Na+ ions.

The molecular dynamics (MD) simulations were carried out by using Nanoscale Molecular Dynamics (NAMD) simulation package that allow high-performance classical simulation of biomolecules in a realistic environment of more than 100,000 atoms (Phillips *et.al.,* 2005). The CHARMM36m (Huang *et.al.,* 2017) force field was used in all simulation systems. The Particle Mesh Edward (PME) was used to treat the long-range electrostatic interactions with a 12.0 Å non-bonded cut off as computing the long-range interaction exactly is not feasible. The energy minimization was performed for 10,000 steps, using the conjugate gradient algorithm. MD simulations were performed for human body temperature 310 K. So, the system was equilibrated for 10 ns taking 1 fs time step and NVT run was propagated for 100 ns of each taking time step 2 fs by using Langevin dynamics with a damping constant of 1 ps-1 for all the temperature.

The NAMD energy plugin package available in Visual Molecular Dynamics (VMD) (Humphrey *et.al.,* 1996) was used to deal structural activity; model building as well as trajectory analysis of the protein and ligand complex.

CHAPTER 4

RESULT AND DISCUSSION

4.1 Selection of protein targets

The development of uterine fibroids, characterized by excessive menstrual bleeding known as menorrhagia, involves the aberrant activation of the Wnt/β-catenin signaling pathway. Sharan et al. (2011) suggest that leiomyoma stem/progenitor cells interact with mature myometrial or leiomyoma cells via this pathway, promoting fibroid growth. Moreover, estrogen-induced overexpression of aromatase, mediated by DVL3 protein, further exacerbates fibroid development and menorrhagia.

In the absence of Wnt ligands, a destruction complex, including GSK-3 β, Axin II, APC, and CK1, degrades β-catenin, preventing signal transduction (Sharan et al., 2011). Conversely, upon Wnt activation, β-catenin accumulates in the nucleus, leading to the transcriptional activation of various genes involved in cell cycle regulation and maintenance of undifferentiated phenotypes.

Wnt ligands undergo PORCN-dependent palmitoylation, essential for their secretion and signaling activity (Sharan et al., 2011). Inhibitors targeting PORCN prevent Wnt ligand secretion, thus attenuating downstream signaling. Additionally, DVL plays a crucial role in Wnt signal transduction by recruiting components of the β-catenin destruction complex to the cell membrane and preventing its assembly (Sharan et al., 2011).

Axin acts as a scaffold protein in the Wnt signaling pathway, regulating cellular functions by interacting with Dvl and β-catenin (Schwarz-Romond et al., 2007b). Targeting the DIX domain of Axin may prevent its interaction with Dvl, thus inhibiting aberrant Wnt signaling and reducing fibroid size (Choi et al., 2010; Fiedler et al., 2011).

Overall, dysregulation of the Wnt/β-catenin cascade contributes to uterine fibroid development and progression. Intervention targeting proteins involved in this pathway, such as PORCN, DVL, and Axin, presents a promising approach for therapeutic intervention in uterine fibroids (Sharan et al., 2011).

4.2 Retrieval and validation of 3D structure of Protein

4.2.1 Retrieval of 3D structure of target proteins

In scientific endeavors, understanding the three-dimensional structures of biological macromolecules is paramount for devising innovative diagnostic and therapeutic approaches. The Protein Data Bank (PDB), particularly through the RCSB Protein Data Bank, serves as a pivotal global repository for atomically detailed structural data, facilitating research across diverse domains including structural and computational biology. Accessible tools for structural analysis and visualization offered by the RCSB PDB empower users to explore intricate molecular mechanisms and expedite the identification of potential drug targets. (Altunkaya et al., 2016; Bajorath, 2002).

In our study, we utilized the crystal structures of the following proteins for molecular docking procedures:

Table 3: Crystal Structures Used for Molecular Docking in the Study

Protein Name	**PDB ID**
PORCN	7URD
PDZ domain of DVL	2KAW
DEP domain of DVL	5LNP
DIX domain of DVL	6JCK
DIX domain of AXIN	6JCK

4.2.2 Structure Validation of retrieved proteins

Assessing the accuracy and reliability of protein structure models is crucial prior to computational drug discovery experiments (Berman et al., 2006). Key requirements include correct stereochemistry, evaluated using tools like PROCHECK and WHATCHECK, which detect anomalies such as steric collisions and unfavorable bond geometry (Bhattacharya et al., 2007). Ramachandran plot analysis is employed to identify unrealistic conformations, with 90% of residues ideally falling within permissible regions (Laskowski, 1993). Additional scrutiny can be applied using servers like SAVES v5.0 for comprehensive assessment

(https://prosa.services.came.sbg.ac.at/prosa.php). In the analysis of our protein crystal structure, over 90% of residues fell within permissible regions.

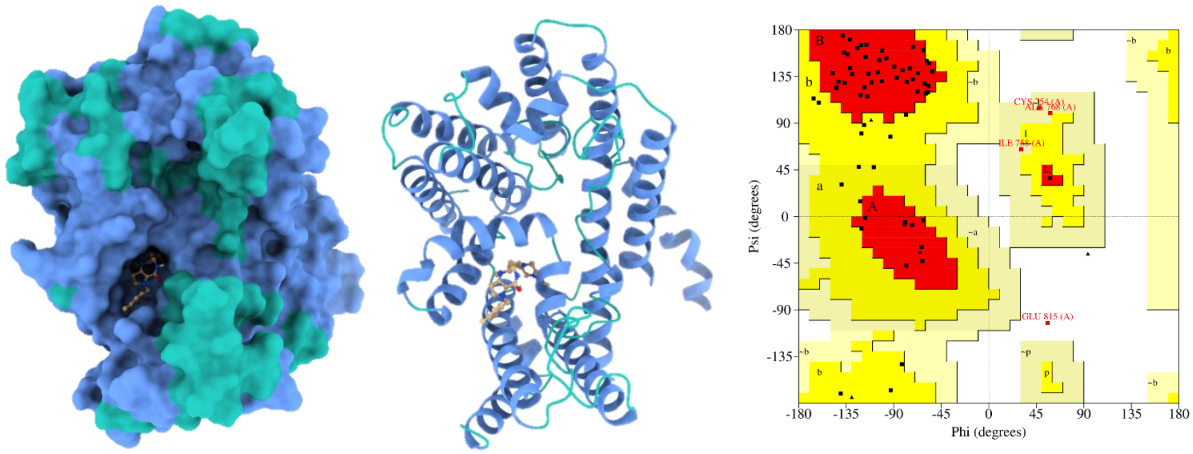

Fig 7: PORCN target protein (7URD) surface and cartoon structure and Ramachandran plot

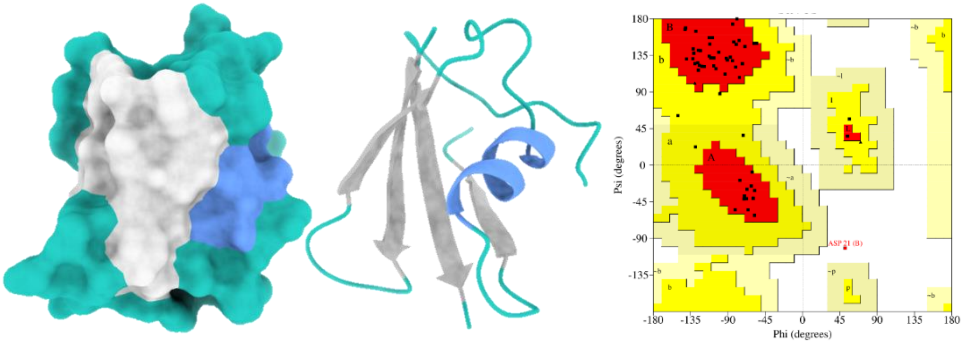

Fig 8: PDZ domain of DVL (2KAW) surface and cartoon structure and Ramachandran plot

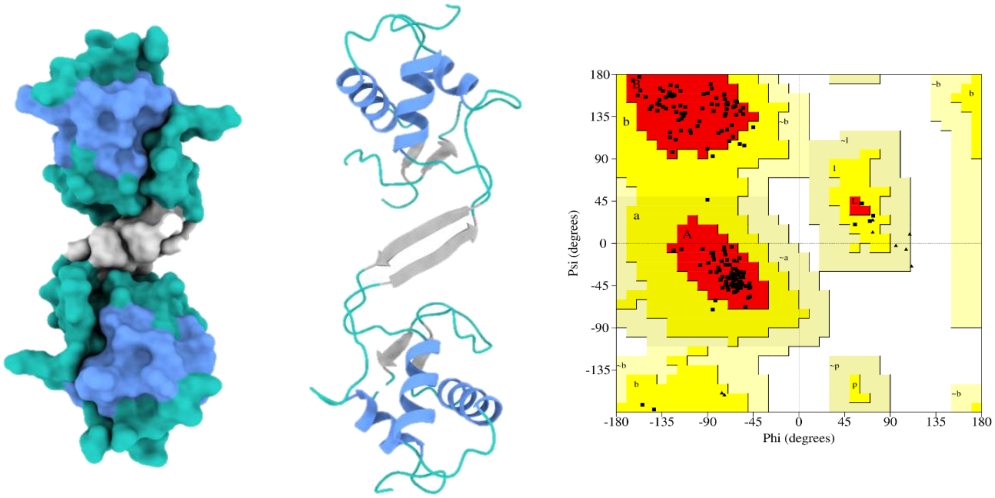

Fig 9: DEP domain of DVL (5LNP) surface and cartoon structure and Ramachandran plot

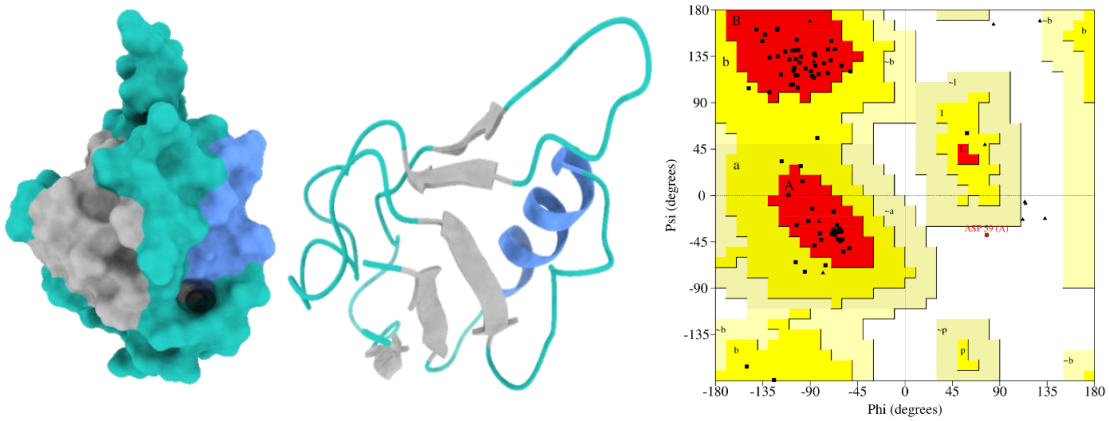

Fig 10: DIX domain of DVL (6JCK) surface and cartoon structure and Ramachandran plot

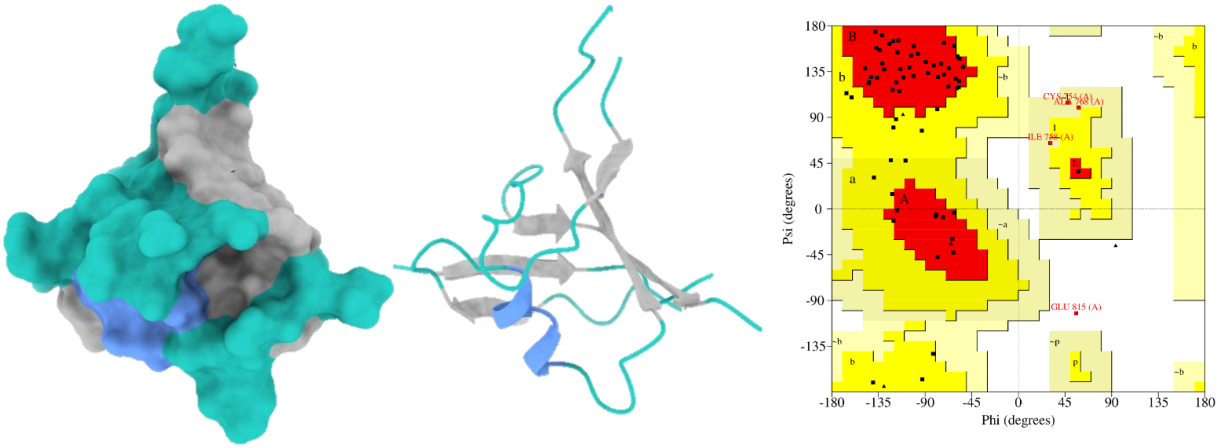

Fig 11: DIX domain of AXIN (6JCK) surface and cartoon structure and Ramachandran plot

4.3 Molecular docking simulation

4.3.1 Target protein preparation

The crystal structure selected for molecular docking procedures in our study was PORCN (PDB id: 7URD), PDZ domain of DVL (PDB id: 2KAW), DEP domain of DVL (PDB id: 5LNP), DIX domain of DVL (PDB id: 6JCK) and DIX domain of AXIN (PDB id: 6JCK). was obtained from Protein Data Bank (rcsb.docking.org) in PDB format.

In preparing proteins for docking simulations using PyRx's Autodock Vina tool, converting PDB to Pdbqt format is essential, involving deletion of water molecules and addition of hydrogen atoms (Wong et al., 2010). This ensures computational ease and clears potential binding pockets. Preservation of water molecules only occurs if they contribute significantly to binding interactions. Hydrogen bond identification is crucial for stabilizing protein-ligand complexes, requiring precise hydrogen atom positioning due to their high mobility (Lippert et al., 2009). Addressing crystallographic ambiguities and adding hydrogen atoms are imperative before structure-based calculations, especially in X-ray crystallography-derived structures.

Merging non-polar bonds is also performed to enhance accuracy (Berman et al., 2000). Accurate partial charges on protein and ligand are crucial for precise complex geometry and binding energy estimation, with different methods yielding varying results. Gasteiger charges, based on electronegativity equilibration, are commonly utilized for this purpose (Dunitz et al., 1994; Tsai et al., 2008; Bikadi et al., 2009).

4.3.2 Ligand Library Preparation

4.3.2.1 Ligand database selection

In the preparatory phase of molecular docking, constructing a ligand database is pivotal. The selection of suitable ligand groups poses a critical decision between chemical synthesis and natural compounds. Chemical synthesis libraries offer established functionalities like kinase inhibitors and indole scaffolds, albeit with intricate filtering challenges and the risk of competitive inhibition.

On the contrary, natural product (NP) libraries, such as those sourced from the ZINC database, present an increasingly vital resource in modern pharmacology, with over 50% of recent drug developments stemming from NPs. The ZINC database, housing more than 20 million molecules in physiologically relevant representations, provides a rich repository for ligand exploration and selection (Newman & Cragg, 2016; Irwin et al., 2012). For our investigation, 224,205 natural product ligands were procured from the Zinc 15 database in sdf file format.

4.3.2.2 In-silico ADME/Tox Tests

In drug discovery, the rigorous process of identifying and developing new compounds is hindered by challenges such as unfavorable pharmacokinetic characteristics and toxicity risks. To address this, predictive tools like OSIRIS aid in assessing ligands for essential parameters such as molecular weight, lipophilicity, solubility, and pharmacokinetic features. Adhering to criteria like Lipinski's rule of five, these tools help anticipate a compound's drug-likeness and toxic profiles, thus guiding the selection of promising lead molecules for further development (Mandlik et al., 2016).

Table 4: Selection Criteria for Drug-like Ligands: Molecular Descriptor Ranges

Properties	Range	Unit
Total Molecular Weight	200 to 500	Dalton
Clog P	-3 to 6	
Clog S	-4 to -2	
H acceptor	0 to 10	
H donor	0 to 5	
Polar Surface Area	0 to 120	$Å^2$
Druglikeness	Positive value	
Rotable bond count	0	

Table 5: Toxicity Assessment Criteria

Properties	Level
Mutagenesis	None
Reproductive effects	None
Tumorigenicity	None
Irritant	None

The successful development of pharmaceutical drugs relies on several crucial physicochemical properties to ensure optimal absorption, distribution, and effectiveness within the body. Hydrophilicity, often indicated by a compound's logP value, plays a significant role in its absorption potential, with lower logP values indicating better absorption. Lipophilicity, on the other hand, affects various aspects of a drug's behavior within the body, such as receptor binding and blood-brain barrier penetration (Dunning et al., 2012).

Furthermore, water solubility, reflected in cLogS values, is essential for a drug's distribution and overall pharmacological action. Hydrogen bonding within drug molecules influences absorption, with excessive hydrogen bonds hindering the molecule's ability to traverse cellular environments efficiently. Molecular characteristics like Lipinski hydrogen bond donors and

acceptors are calculated based on the presence of OH, NH, nitrogen, and oxygen atoms, providing insights into a compound's hydrogen bonding potential (Li et al., 2011).

Additionally, the number of rotatable bonds reflects molecular flexibility, impacting oral bioavailability (Veber et al., 2002). Polar surface area, primarily consisting of oxygen and nitrogen atoms, influences a drug's ability to cross barriers like the blood-brain barrier. High polar surface area values can hinder a molecule's effectiveness by impeding cellular entry. Drug likeness, assessed through OSIRIS drug scores, provides a qualitative measure of a compound's potential bioavailability and suitability for pharmaceutical use (Pajouhesh Hassan & Lenz, 2005).

Finally, ADMET filters, implemented through OSIRIS, ensure the exclusion of compounds with mutagenic, tumorigenic, irritating, or reproductive effects, resulting in a refined library of 35,834 ligands suitable for further drug design and evaluation.

4.3.2.3 Energy Minimization

In molecular design, various energy components like stretching, bending, and torsion contribute to a molecule's potential energy. The optimization of ligand structures through energy minimization is pivotal to identifying their most stable conformations. Among 35,534 retrieved ligands, 300 were excluded due to potential instability during this energy minimization process. Consequently, the remaining compounds have been earmarked as the primary library for potential drug candidates.

4.3.2.4 Filtration of Primary Ligand Library: hMAT1A as reference protein

S-adenosyl methionine synthetase, also known as MAT, is a pivotal enzyme in humans responsible for synthesizing SAM, a vital methyl group donor crucial for various biological processes including polyamine and glutathione synthesis (Lu et al., 2008; Mato et al., 1997). MAT facilitates this process by transferring the adenosyl group from ATP to the sulfur atom of L-methionine, cleaving the ATP triphosphate chain at both ends (Shafqat et al., 2013).

In a recent study, molecular docking of a primary ligand library comprising 35,534 compounds against human MAT1A revealed that compounds exhibiting stronger binding affinity than the native ligand SAM were excluded, resulting in a refined pool of 11,970 ligands.

4.3.2.5 Further narrowing down: CYP3A4 as reference protein

After molecular docking, the library of 11,970 compounds was examined for their ability to

inhibit RIT, using CYP3A4 and any compounds that had a greater affinity for binding than the native ligand RIT were excluded. 9,977 ligands remained from a library of 11,970 ligands.

4.3.2.6 Active site/Binding pocket identification

The ligand binding sites or pocket of the protein PORCN and PDZ domain of DVL were identified from the crystal structure of PDB id: 7URD and 2KAW respectively, available in RCSB protein data bank. The active sites for these proteins were further verified by taking the amino acid residues of the protein within 5 A of reference inhibitor bound in PYMOL. The active sites from the RCSB protein data bank were found in consistent with active sits derived from PYMOL software.

While the active site of the DIX and DEP domain of DVL, and DIX domain of AXIN were generated using PYMOL, by analyzing the interacting residues between the protein interfaces, to which we call interaction mapping. Therefore, using this feature of PYMOL, we can identify the important interacting residues between the protein interfaces and use for molecular docking.

The DVL protein interacts with AXIN via heterotypic DIX-DIX interaction and thereby triggering the Wnt signal transduction. Mapping the interaction between this interfaces, active site for DIX domain of each protein DVL and AXIN were identified. The interacting residues were identified from the crystal structure available in RCSB protein data bank with PDB id 6JCK.

Similarly, DEP dimerization of DVL protein is one of the crucial step in assembly of functional signalosome. Targeting the interface between this homodimer formations between the DEP domains of two DVL protein serve as a good sit for active site identification for molecular docking. With this in mind the active site for DEP domain were identified using interaction mapping via PYMOL. The interacting residues were identified from the crystal structure available in RCSB protein data bank with PDB id 5LNP.

4.3.3 Virtual screening of the final ligand library

For screening of potential drug candidate, molecular docking of prepared ligand library (Natural product and Biogenic) as per requirement was performed against the target proteins along with their reference inhibitor was performed in PyRx platform.

PORCN as protein target

Molecular docking of natural product and biogenic library long with the reference inhibitor LGK 974 against PORCN (7URD) was performed, with parameter set to 32 as number of modes and exhaustiveness. This gave 2 molecules each from natural product and biogenic library having binding energy higher than that of reference ligand. Such higher binding affinities of natural product and biogenic indicated that there could be competitive inhibition of the target proteins by the selected ligands.

PDZ domain of DVL as protein target

On docking natural product along with the reference inhibitor, against PDZ domain of DVL (2KAW) gave a total of 115 molecules having binding energy greater than that of inhibitor molecules, suggesting higher binding affinities towards 2KAW than inhibitor molecule.

DEP domain of DVL as protein target

Molecular docking of natural product along with the reference inhibitor as performed against DEP-DEP interface of DVL (5LNP), which gave 71 molecules having binding energy higher than that of native reference inhibitor, suggesting higher binding affinities toward 5LNP than the reference inhibitor.

DIX domain of DVL as protein target

A total of 48 molecules were screened with binding energy higher than that of reference inhibitor molecules, on docking against DIX domain of DVL (6JCK). It provided an insight that the screened molecules has better binding affinities toward 6JCK than the reference inhibitor taken into consideration.

DIX domain of AXIN as target

On docking natural product along with the reference inhibitor, against DIX domain of AXIN, gave a total of 127 molecules with binding energy greater than the inhibitor suggesting the higher binding affinities towards DIX domain of AXIN than inhibitor molecule.

Such higher binding affinities of the prepared ligand library toward the protein target indicated that there could be competitive inhibition of the target proteins by the selected ligands, which also need further processing to develop into potential lead like molecules.

4.3.4 Screening with Phase I drug filter: Involvement in drug filter

The hepatic cytochrome P450 (CYP) enzymes play a vital role in metabolizing various drugs and xenobiotics, with each isozyme reacting differently to external substances. Certain CYP isozymes, such as CYP 1A1 and CYP 1A2, are implicated in the activation of carcinogens, leading to DNA damage and potentially carcinogenesis. Moreover, other CYP enzymes like CYP 3A and CYP 2E1 can convert existing carcinogens into highly mutagenic compounds. Consequently, the stimulation of these CYP isozymes is linked to the carcinogenic potential of various substances (Sheweita, 2000).

In drug discovery, molecules with superior binding affinities against target proteins, including PORCN, PDZ, DEP, and DIX domains of DVL and AXIN, were screened. These molecules were further docked with hepatic cytochrome P450 enzymes (CYP1A1, CYP1A2, CYP1B1, CYP2C9, CYP2C19, CYP2D6, and CYP2E1). Compounds exhibiting weaker binding affinities compared to reference inhibitors were selected for further investigation to ensure they do not disrupt drug metabolism and other essential bodily functions governed by these enzymes, facilitating the safe clearance of drugs and compounds within the body.

4.3.5 Screening of top hits: Based on Preference index and docking results

In this study, ligands lacking inhibitory effects on phase I drug metabolizing enzymes were assessed for their binding affinity to hMAT1A and hCYP3A4, crucial enzymes in human physiology. To identify potential drug candidates with reduced enzyme inhibition, an empirical formula incorporating H-bond acceptor, H-bond donor, and rotatable bond counts was utilized to calculate a preference index mimicking molecule permeability and residence time in protein active sites. This approach, based on principles outlined by Schwöbel et al. (2011), emphasizes the importance of H-bond interactions in crossing biological membranes and the impact of rotatable bonds on drug residence time. The preference index aids in selecting compounds with optimal residence times, crucial for effective pharmacodynamics, as highlighted by Miller et al. (2012) and Pan et al. (2013).

Of the 4 top hits obtained against PORCN protein target, it was narrowed down to 2 hits, while 115 hits obtained against PDZ domain of DVL was narrowed down to hits. Similarly, 6 hits for DEP domain of DVL, 4 hits for DIX domain of DVL and 7 hits for DIX domain of AXIN protein target was narrowed down from a pool of 71, 115, 48 and 127 hits respectively and tabulated in table

4.3.6 DFT analysis of top hits

DFT is a computational quantum mechanical modeling technique used to examine the electronic structure of atoms, molecules, and solids as well as to look at the interactions between receptors and ligands (van Mourik et al., 2014; Jordaan et al., 2020).

4.3.7 Total energy and Dipole moment

To evaluate the stability of the top lead compounds, their optimized geometries were computed using Gaussian software at the B3LYP/6-31G level of theory. This process involved energy evaluations to determine the total energy at specific stationary points. It serves as a key indicator of molecular stability, guides geometry optimization processes, aids in understanding reaction mechanisms, and provides a basis for calculating various thermodynamic and kinetic properties. Accurate total energy calculations are essential for reliable predictions and insights into molecular behavior and interactions (Wojciechowski et al., 2014; Ioakimidis et al., 2008).

The dipole moment, a key parameter influencing chemical and physical properties, was also assessed due to its significance in drug discovery. Compounds with higher dipole moments typically exhibit greater water solubility and lower absorption through lipophilic membranes, making the dipole moment a valuable metric for predicting cell permeability and oral bioavailability of drugs (Ioakimidis et al., 2008; Matuszek et al., 2016).

4.3.8 Molecular orbital properties

Density Functional Theory (DFT) analysis was used to calculate the Highest Occupied Molecular Orbital (HOMO) and Lowest Unoccupied Molecular Orbital (LUMO) energies to assess chemical reactivity. The HOMO energy indicates regions in small molecules that can donate electrons during complex formation, while the LUMO energy shows the molecule's ability to accept electrons from a protein partner (Banavath et al., 2014). The HOMO-LUMO gap, representing the electronic excitation energy, is crucial for determining the reactivity and stability of compounds (Zheng et al., 2013). The computed HOMO-LUMO gap energies are tabulated.

4.3.9 Narrowing down of top hits into potential lead compound

In order to further screen the potential lead compound, all the top hits targeted for different proteins were analyzed based on the docking result with target protein, hMAT1A, hCYP3A4,

preference index and thermochemical studies (total energy, dipole moment, RMSD and HOMO-LUMO gap) from the DFT calculation.

Table 6: Binding energies of screened ZINC ligands, total energy, dipole moment, RMSD and energy gap, against protein PORCN

Ligand	**B.E (Kcal/mol)**			**P.I**	**T.E**	**D.M**	**RMSD**	**E.G**
Natural Product	PORCN	hMAT1A	hCYP3A4		Kcal/mol	Debye	Hatree/Bohr	kcal/mol
17752	-11.8	-7.1	-9.2	2.4	-877885.94	4.8649	0.0000007	87.236386
Biogenic								
42151	**-12.2**	**-6.9**	**-9.2**	**2.6**	**-984167.24**	**8.2392**	**0.0000002**	**102.82372**

B.E : Binding Energy, P.I: Preferential Index, T.E: Total Energy, D.M: Dipole moment, E.G: Energy gap

Table 7: Binding energies of screened ZINC ligands, total energy, dipole moment, RMSD and energy gap, against PDZ domain of DVL

Ligand	**B.E (Kcal/mol)**			**P.I**	**T.E**	**D.M**	**RMSD**	**E.G**
Natural Product	DVL	hMAT1A	hCYP3A4		Kcal/mol	Debye	Hatree/Bohr	kcal/mol
31802	**-7.5**	**-6.9**	**-9.1**	**1.8**	**-903118.10**	**2.64**	**0.000002**	**119.55**
5855	-7.4	-7.1	-9	2.4	-815574.24	7.67	0.004538	37.39
31537	-7.4	-7	-9.1	2.2	-762091.59	5.23	7.19E-06	147.59
11071	**-7.4**	**-6.9**	**-9.2**	**2**	**-759688.23**	**5.47**	**0.002098**	**90.74**
742	-7.4	-7.1	-9.2	1.4	-612522.79	1.75	0.000006	146.28

B.E : Binding Energy, P.I: Preferential Index, T.E: Total Energy, D.M: Dipole moment, E.G: Energy gap

Table 8: Binding energies of screened ZINC ligands, total energy, dipole moment, RMSD and energy gap, against DEP domain of DVL

Ligand	B.E (Kcal/mol)			P.I	T.E	D.M	RMSD	E.G
Natural Product	DVL	hMAT1A	hCYP3A4		Kcal/mol	Debye	Hatree/Bohr	kcal/mol
18891	**-8.2**	**-6.6**	**-9.6**	**1.2**	**-887645.21**	**3.6**	**0.00000249**	**107.93**
32340	-8.2	-7	-10.2	2.4	-1141380.7	4.9	0.00001134	89.56
1765	**-8.1**	**-6.8**	**-8.4**	**1.8**	**-924762.9**	**3.9**	**0.000002**	**105.34**
7526	-8.1	-6.9	-8.1	2.6	-743497.41	4.4	0.000002	59.43
22065	-8	-6.2	-7.5	1.4	-600192.90	4.0	0.00000223	92.82
25952	-8	-7.1	-10.1	3	-972976.4	5.4	0.000453	118.93

B.E : Binding Energy, P.I: Preferential Index, T.E: Total Energy, D.M: Dipole moment, E.G: Energy gap

Table 9: Binding energies of screened ZINC ligands, total energy, dipole moment, RMSD and energy gap, against DIX domain of DVL

Ligand	B.E (Kcal/mol)			P.I	T.E	D.M	RMSD	E.G
Natural Product	DVL	hMAT1A	hCYP3A4		Kcal/mol	Debye	Hatree/Bohr	kcal/mol
20636	-6.1	-7	-8.8	2.2	-803278.04	8.9075	7.92E-06	121.73
15966	**-6**	**-6.4**	**-8.3**	**2.6**	**-791874.60**	**5.298493**	**0.000007**	**37.16**
6736	**-6**	**-6.8**	**-8.5**	**2.6**	**-995134.43**	**9.678325**	**0.000002**	**109.87**
21486	-6	-6.6	-8.9	2	-735063.38	4.369985	0.000005	113.51

B.E : Binding Energy, P.I: Preferential Index, T.E: Total Energy, D.M: Dipole moment, E.G: Energy gap

Table 10: Binding energies of screened ZINC ligands, total energy, dipole moment, RMSD and energy gap, against DIX domain of AXIN

Ligand	**B.E (Kcal/mol)**			**P.I**	**T.E**	**D.M**	**RMSD**	**E.G**
Natural Product	AXIN	hMAT 1A	hCYP3 A4		Kcal/mol	Debye	Hatree/Bohr	kcal/mol
18457	-6.2	-7.1	-9.2	3	-969725.09	6.11	1.51E-06	106.48
32340	-6.5	-7	-10.2	2.4	-1141377.2	4.90	1.42E-06	82.41
16424	-6.1	-7.1	-9	1.8	-708443.09	3.65	3.95E-06	55.47
13862	-6	-7.1	-8.6	1.8	-961997.23	3.61	3.2E-06	31.41
18023	**-6**	**-6.9**	**-9.5**	**1.8**	**-683503.46**	**4.46**	**0.000002**	**110.88**
31802	**-6**	**-6.9**	**-9.1**	**1.8**	**-903126.91**	**2.22**	**0.000002**	**127.61**
11678	-6.1	-7	-8.5	1.6	-551950.07	3.54	0.000003	79.64

B.E : Binding Energy, P.I: Preferential Index, T.E: Total Energy, D.M: Dipole moment, E.G: Energy gap

Thus, narrowed hits were then were compared between the binding energies target protein and the hits interaction with hMAT1A and hCYP3A4 protein such that the ligands selected might not show any of competitive reaction between this reference proteins. Such that the narrowed potential lead compound would not interfere with the function of the reference proteins (hMAT1A and hCYP3A4). Similarly, further analysis of ligands total energy conferring its stability, dipole moment, RMSD and energy gap suggesting for its reactivity with the docked proteins, narrowed hits with green color are suspected as potential lead compound.

4.4 Protein-Ligand Interaction

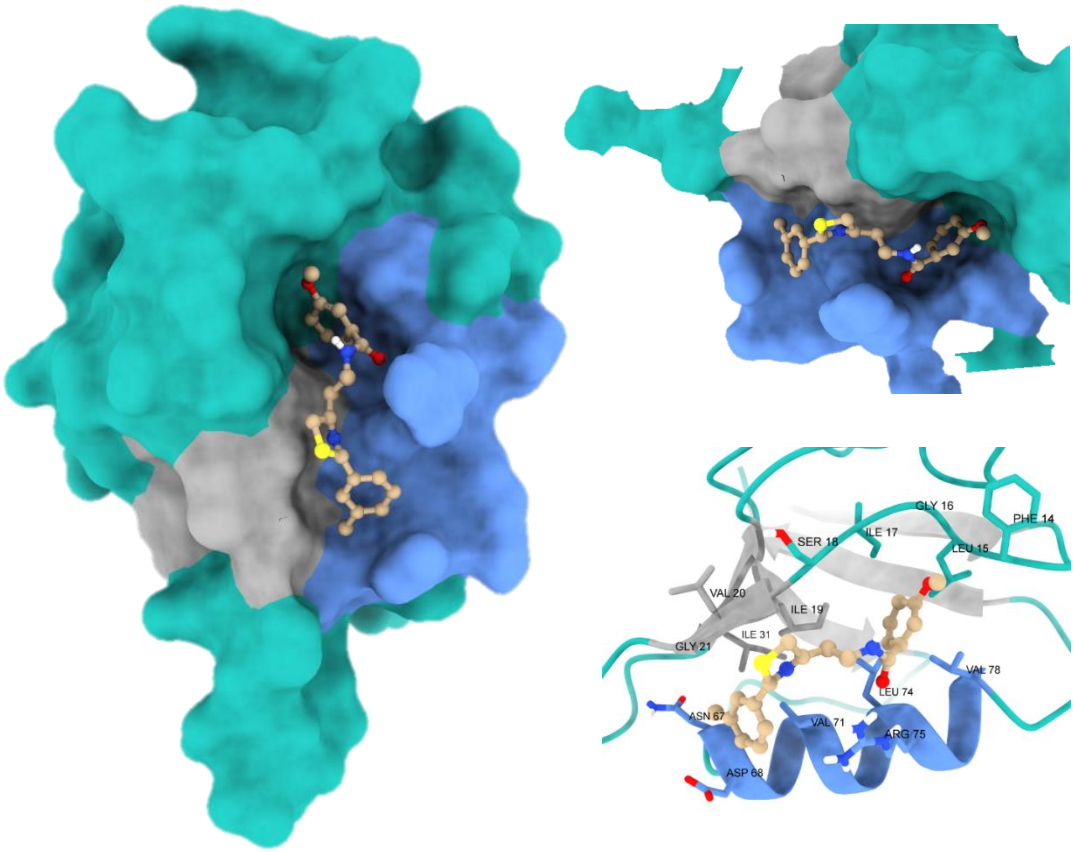

Fig12: Protein ligand complex after docking and amino acids residues within 5 A of compound 31802 against PDZ domain of DVL target protein.

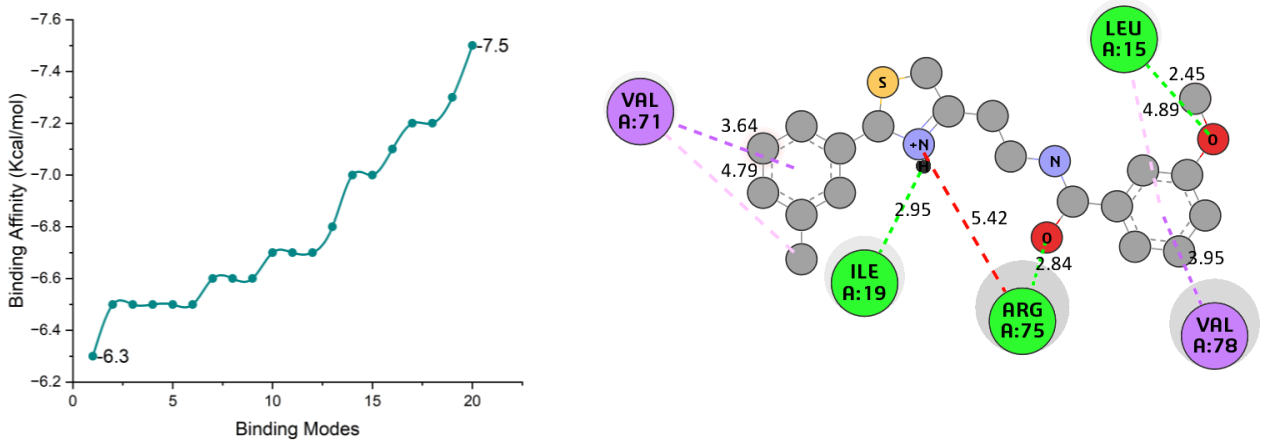

Fig 13: 20 different binding modes calculated via docking, with optimizing the docking energy to best suit docking pose and its respective binding affinity. 2D interaction of ligand with protein residues.

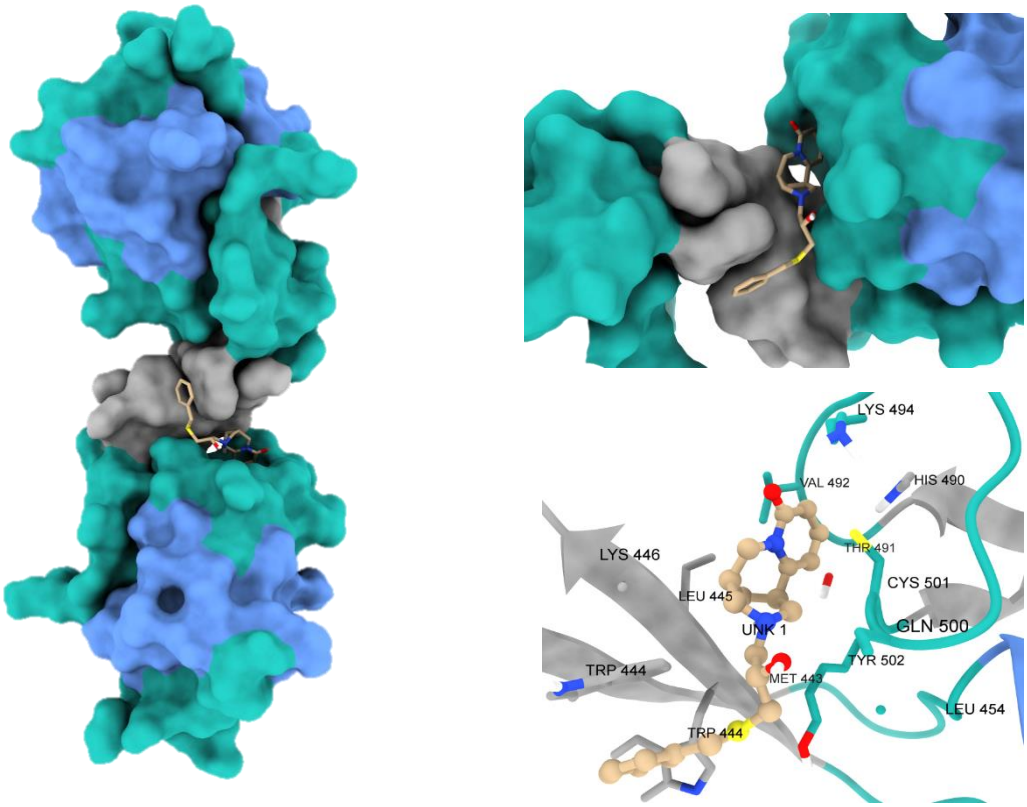

Fig 14: Protein ligand complex after docking and amino acids residues within 5 A of compound 1765 against DEP domain of DVL target protein.

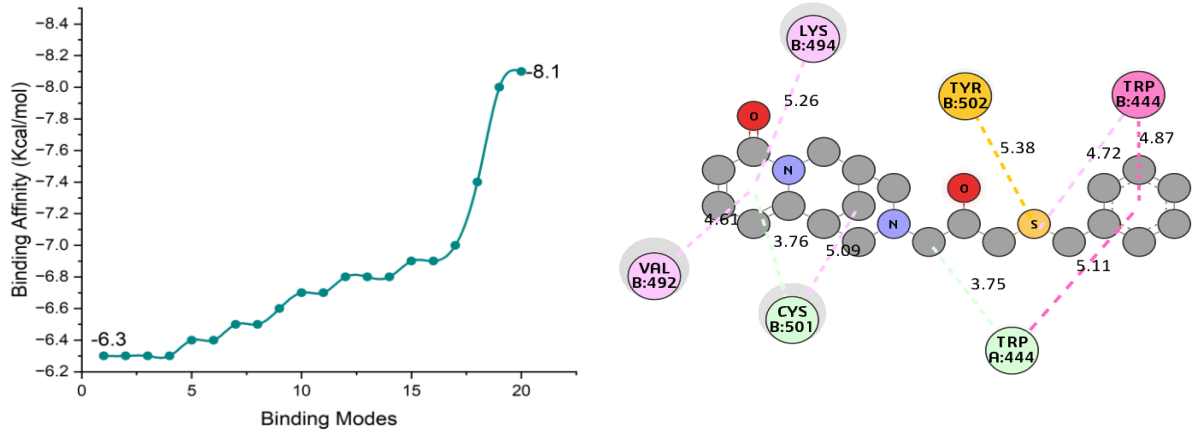

Fig 15: 20 different binding modes calculated via docking, with optimizing the docking energy to best suit docking pose and its respective binding affinity. 2D interaction of ligand with protein residues.

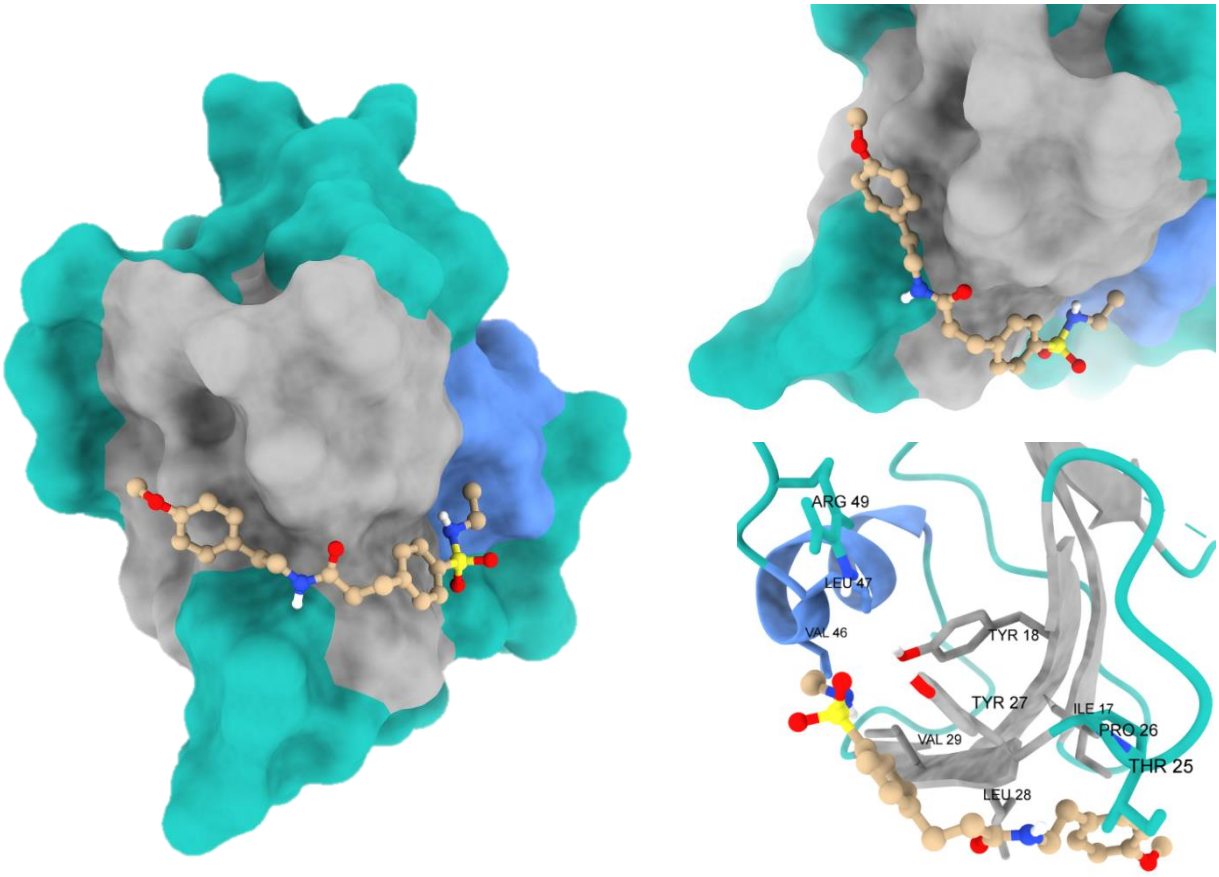

.

Fig 16: Protein ligand complex after docking and amino acids residues within 5 A of compound 6736 against DIX domain of DVL target protein.

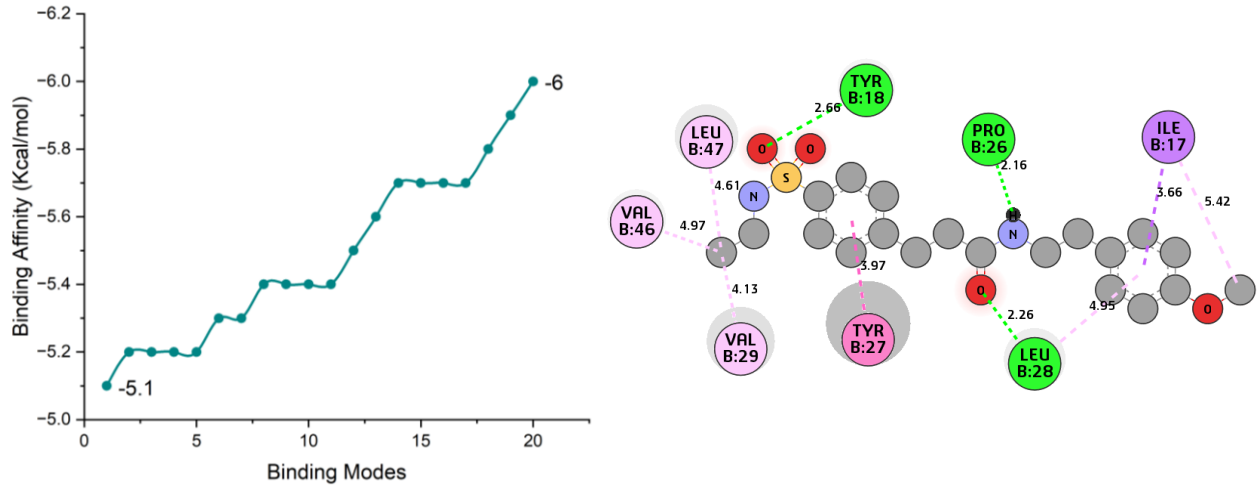

Fig 17: 20 different binding modes calculated via docking, with optimizing the docking energy to best suit docking pose and its respective binding affinity. 2D interaction of ligand with protein residues.

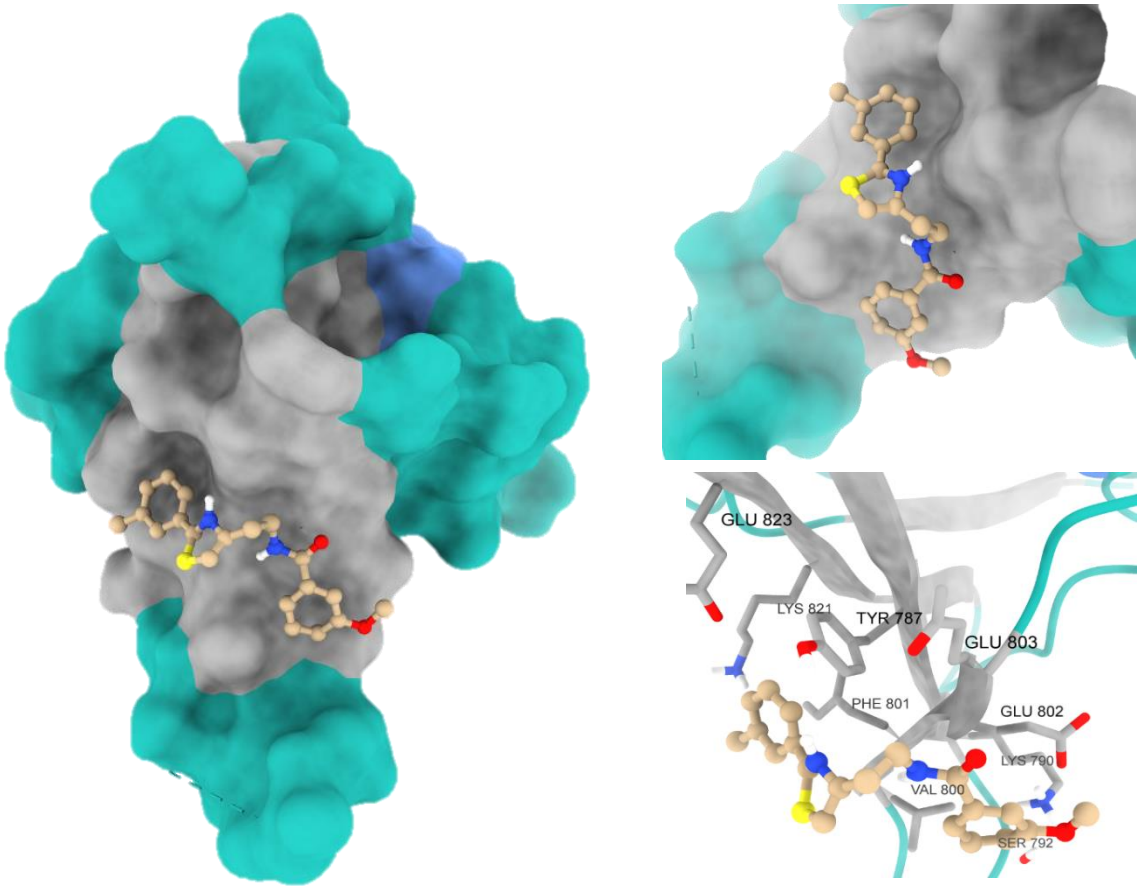

Fig 18: Protein ligand complex after docking and amino acids residues within 5 A of compound 31802 against DIX domain of AXIN target protein

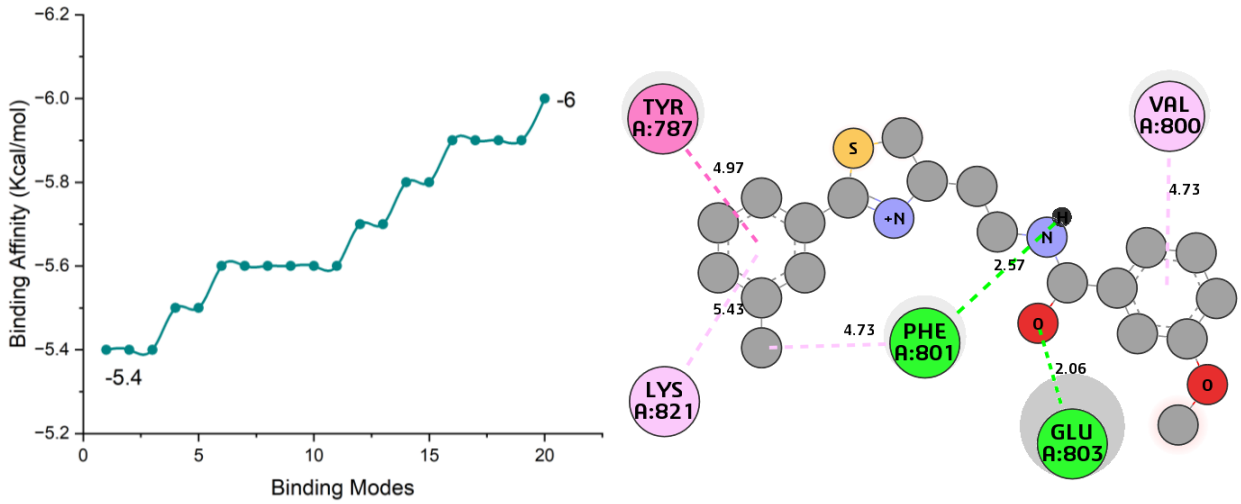

Fig 19: 20 different bindings modes calculated via docking, with optimizing the docking energy to best suited docking pose and its respective binding affinity. 2D interaction of ligand with protein residues.

It's evident that the docked molecules have seamlessly integrated into the active site groove. Visualizing the binding of the ligand to specific amino acids and the subsequent reorientation of these amino acids in the active sites can be achieved through ChimeraX. In the figure

provided for ligands 42151, 31802, 1765, 6736, and 31802, amino acid residues within a 5 Å diameter from the ligand-bound state are depicted. This clearly demonstrates that the calculated binding energies for these ligands against PORCN, PDZ domain of DVL, DEP domain of DVL, DIX domain of DVL, and DIX domain of AXIN respectively, correspond to the binding of the ligands to the amino acid residues within the active site. Consequently, protein-ligand interactions can be thoroughly analyzed to understand the nature of ligand-protein binding.

To analyze the protein-ligand interaction, Biovia Discovery Studio was used. The 2D interactions of these complexes were analyzed Biovia Discovery Studio (Baskaran *et.al.*, 2020). Upon analyzing the protein-ligand interaction after molecular docking in Biovia Discovery Studio, the bonds mainly involved were found to be hydrogen bond, Pi-alkyl, Pi-Sigma, P-Pi T-shaped, alkyl, Pi-sulfur. These bond types and the bond length present in the maceomolecule imply the respective bindig energy calculated while docking. The type of bond and the bond length are tabulated in the table below.

Table 11: Binding nature of compound 42151 at active site of PORCN visualized in Biovia Discovery studio

Chain	Amino acid	Bond type	Bond category	Bond length (Å)
A	TYR329	Conventional Hydrogen Bond	Hydrogen Bond	2.38292
A	SER332	Conventional Hydrogen Bond	Hydrogen Bond	2.23491
A	TYR329	Carbon Hydrogen Bond	Hydrogen Bond	3.65696
A	HIS357	Pi-Sigma	Hydrophobic	5.12342
A	VAL296	Pi-Pi Stacked	Hydrophobic	5.42572
A	LEU349	Alkyl	Hydrophobic	5.1147
A	VAL325	Alkyl	Hydrophobic	5.31731
A	TRP300	Alkyl	Hydrophobic	4.38394
A	TRP300	Pi-Alkyl	Hydrophobic	4.25962
A	TYR354	Pi-Alkyl	Hydrophobic	4.90533
A	HIS357	Pi-Alkyl	Hydrophobic	4.15187
A	VAL294	Pi-Alkyl	Hydrophobic	5.33976

A	VAL325	Pi-Alkyl	Hydrophobic	4.7123

Table 12: Binding nature of compound 1765 at active site of DEP domain of DVL visualized in Biovia Discovery studio

Chain DEP	**Amino acid**	**Bond type**	**Bond category**	**Bond length (Å)**
A	TRP444	Carbon Hydrogen Bond	Hydrogen Bond	3.75294
B	CYS501	Pi-Donor Hydrogen Bond; Pi-Sulfur	Hydrogen Bond; Other	3.75591
B	TYR502	Pi-Sulfur	Other	5.37593
B	TRP444	Pi-Pi Stacked	Hydrophobic	3.94647
B	TRP444	Pi-Pi Stacked	Hydrophobic	3.69234
A	TRP444	Pi-Pi T-shaped	Hydrophobic	5.10509
B	CYC501	Alkyl	Hydrophobic	5.09032
B	TRP444	Pi-Alkyl	Hydrophobic	4.71824
B	VAL492	Pi-Alkyl	Hydrophobic	4.60826
B	LYS494	Pi-Alkyl	Hydrophobic	5.25931

Table 13: Binding nature of compound 6736 at active site of DIX domain of DVL visualized in Biovia Discovery studio

Chain	**Amino acid**	**Bond type**	**Bond category**	**Bond length (Å)**
B	TYR18	Conventional Hydrogen Bond	Hydrogen Bond	2.66354

B	LEU28	Conventional Hydrogen Bond	Hydrogen Bond	2.25629
B	UNK1	Conventional Hydrogen Bond	Hydrogen Bond	2.16308
B	ILE17	Pi-Sigma	Hydrophobic	3.6623
B	TYR27	Pi-Pi Stacked	Hydrophobic	3.96934
B	VAL29	Alkyl	Hydrophobic	4.12984
B	VAL46	Alkyl	Hydrophobic	4.96537
B	LEU47	Alkyl	Hydrophobic	4.60948
B	ILE17	Alkyl	Hydrophobic	5.41657
B	LEU28	Pi-Alkyl	Hydrophobic	4.95289

Table 14: Binding nature of compound 31802 at active site of DIX domain of AXIN visualized in Biovia Discovery studio

Chain	**Amino acid**	**Bond type**	**Bond category**	**Bond length (Å)**
A	GLU803	Conventional Hydrogen Bond	Hydrogen Bond	2.05593
A	PHE801	Conventional Hydrogen Bond	Hydrogen Bond	2.57401
A	TYR787	Pi-Pi T-shaped	Hydrophobic	4.97071
A	PHE801	Pi-Alkyl	Hydrophobic	4.73351
A	LYS821	Pi-Alkyl	Hydrophobic	5.4318
A	VAL800	Pi-Alkyl	Hydrophobic	4.72558

Table 15: Binding nature of compound 31802 at active site of PDZ domain of DVL visualized in Biovia Discovery studio

Chain	Amino acid	Bond type	Bond category	Bond length (Å)
A	LEU15	Conventional Hydrogen Bond	Hydrogen Bond	2.44832
A	ARG75	Conventional Hydrogen Bond	Hydrogen Bond	2.84118
A	ILE19	Conventional Hydrogen Bond	Hydrogen Bond	2.95211
A	VAL71	Pi-Sigma	Hydrophobic	3.6403
A	VAL78	Pi-Sigma	Hydrophobic	3.94746
A	VAL71	Alkyl	Hydrophobic	4.78832
A	LEU15	Pi-Alkyl	Hydrophobic	4.88659

4.5 Molecular Electrostatic Potential

Molecular electrostatic potential is fundamentally a measure of the strength of the nearby charges, nuclei and electrons, at a particular position. The shape and size of the molecule are obtained by molecular electrostatic potential (MEP) interms of colors. The value of electrostatic potential is given in terms of distinct colors. The positive region is depicted in blue (a nucleophilic site) for a nucleophilic attack, whereas the negative region is indicated in red (a electrophilic site) for an electrophilic attack and green indicates zero potential areas in the molecule. On surface mapping/arrays, MEP increases in the following order: red, orange, yellow, green, and blue. The MEP diagram of all the potential lead compound is given in figure.

The MEP diagram of compound 31802, a potential lead targeted for protein PDZ domain of DVL is shown in figure above. The negative and positive region of this compound is between -5.94e-2 and +5.94e-2. In this compound, oxygen atom O48 and O56 are more negative and shown in red color. This because of the presence of C=O and partial C=O. The red region represents the site with higher electron density, therefore, able to donate electrons to reacting species. Similarly, N36 and S34showed slightly negative charge with yellow in color. While, hydrogen attached with O48, N46 and N36 are represented by blue color. The remaining portions are green in color, representing zero potential area, in this compound.

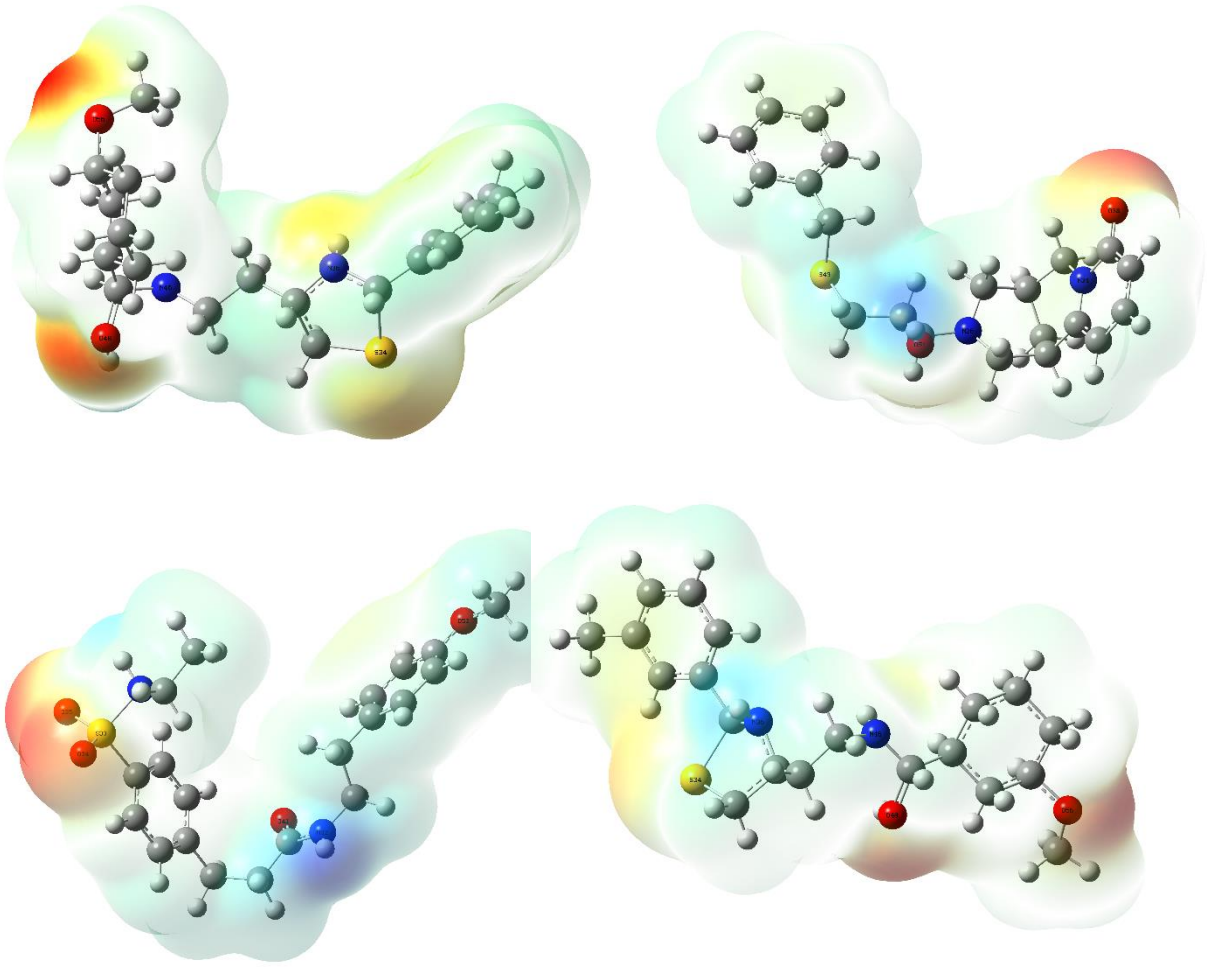

Fig 20: MEP diagram of ligand 31802(top left), 6736 (top right), 1765 (bottom left) and 31802 (bottom right), a potential lead compound targeted against PDZ, DEP, DIX domain of DVL and DIX domain of AXIN. Red regions of the molecule would correspond to areas with the most negative electrostatic potential, which are typically associated with the presence of lone pairs or electron-rich functional groups. Blue regions would correspond to areas with the most positive electrostatic potential, which are typically associated with the presence of positively charged atoms or electron-deficient functional groups. Green regions would correspond to areas with intermediate electrostatic potential values.

Similarly, the MEP diagram of compound 6736 (targeted for protein DIX domain of DVL) is shown in figure above. The negative and positive region is between -7.132e-2 to 7.132e-2. Compound 6736, hs 4 of the oxygen atoms, of which O35 and O34 represent red color whereas O41 showed orange color and O52 represent in yellow color. Similarly, ydrogen attached with N42 shown in blue color, therefore representing positive electrostatic potential. While, remaining portion represent the area with zero potential area.

The electrostatic potential of ligand 1765 (targeted for DEP DEP domain of DVL) lies between -7.686e-2 to 7.686e-2, suggesting their negative to positive region. Looking onto the diagram of the MEP, O38 was shown to have higher electron density than the rest of the atom of the ligand, while O51 and S43 showed negative but depicting less electron density than O38. While, hydrogen atom bonded with O51 showed region with low electron density as identified by blue color. Remaining other interface and atoms showed zero electrostatic potential denoted by greenish color area.

The electro static potential of ligand 31802 targeted for DIX domain of AXIN lies between -5.652e-2 to 5.652e-2 as their negative to positive electrostatic potential with red as negative and blue being positive electrostatic potential. O48 and O56 showing higher electron density therefore, will be involved in electron withdrawing capability between their bonded atom during the chemical reaction of interfering with the protein complex. While, S34 and N46 showed yellowish color therefore, it also exhibit certain electron density but lesser than that of oxygen atom, still it will also help the ligand in interacting further with protein complex. While, hydrogen around the nitrogen atom and hydrogen associated around benzene ring showed bluish color, representing this group being positive electrostatic potential. Remaining interface showed zero electrostatic potential.

With such type of information in relevance with molecular electrostatic potential we can predict further the electronic properties of the interaction as electrophilic or nucleophilic attack or reaction. The red hue represents the negative area and suggests nucleophilic reactivity, whereas the blue color depicts electrophilic reactivity in the positive region of MEP surface plots. These plots are the basis for the understanding and visualization of the relative polarity of the molecule. So the reactive areas of the compound easily identified based on the electron and proton interactions show biological activity.

4.6 Frontier Molecular Orbital Analysis

The most significant orbitals are called frontier molecular orbitals (FMO), and they are crucial in charge transfer interactions with the binding site of the target protein. Understanding reactions and active site conjugations is aided by FMO analysis. These are the Lowest Unoccupied Molecular Orbital and the Highest Occupied Molecular Orbital, LUMO and HOMO respectively. The major orbitals that contribute to the complex's chemical stability are the lowest unoccupied molecular orbital (LUMO) and the highest occupied molecular orbital (HOMO). The active compounds' chemical reactivity and chemical stability are well explained

by the difference in bond energy (Govindarajan et al., 2012). HOMO energy indicates the ability or character of donating electrons and LUMO energy is responsible for accepting the electron. These regions are located over a protein-ligand complex at different locations indicating the charge transfer in LUMO regions.

The HOMO and LUMO region of narrowed ligand targeted for each ligand is shown in figure.

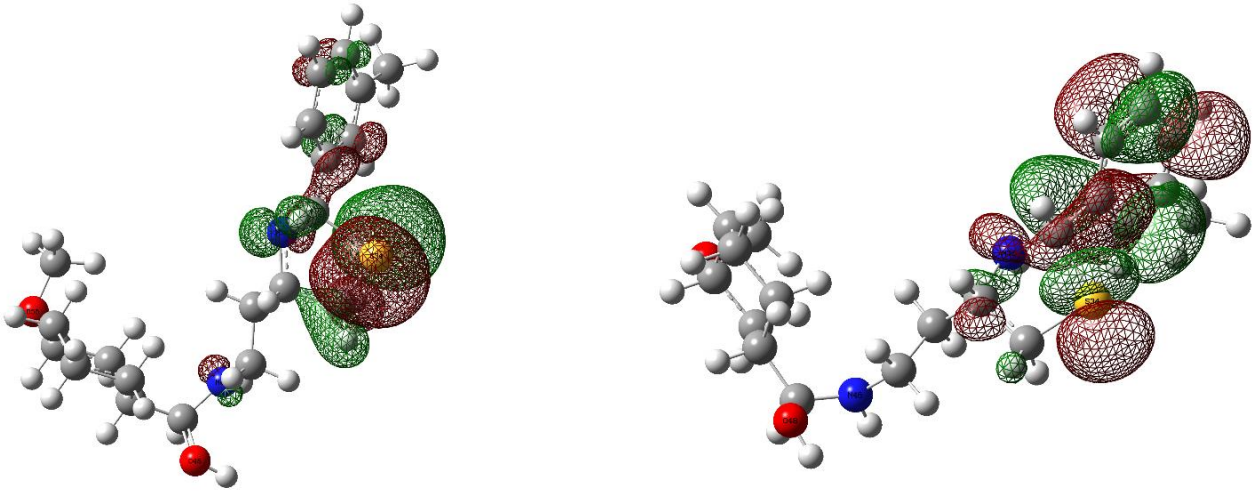

Fig 21: Frontier molecular orbital of compound 31802 (PDZ domain of DVL)

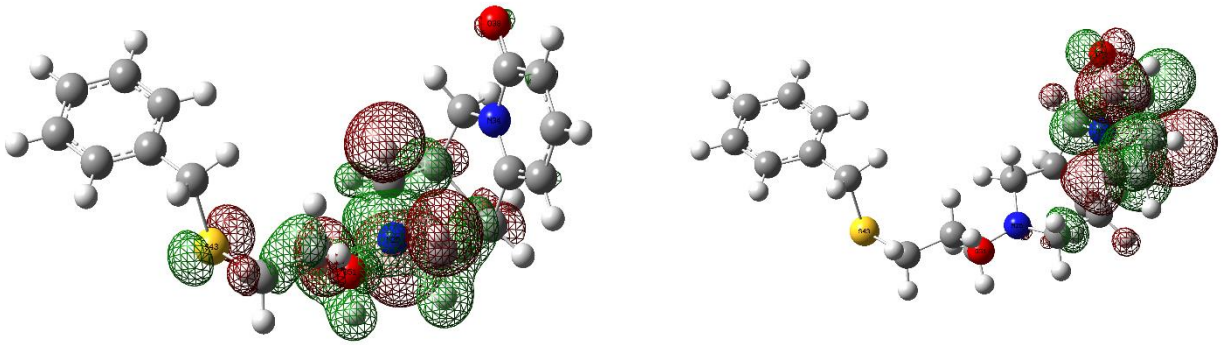

Fig 22: Frontier molecular orbital of compound 1765 (DEP domain of DVL)

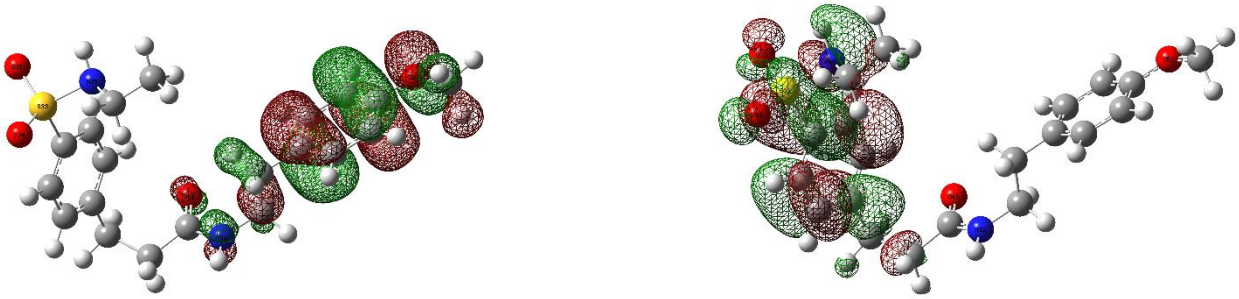

Fig 23: Frontier molecular orbital of compound 6736 (DIX domain of DVL)

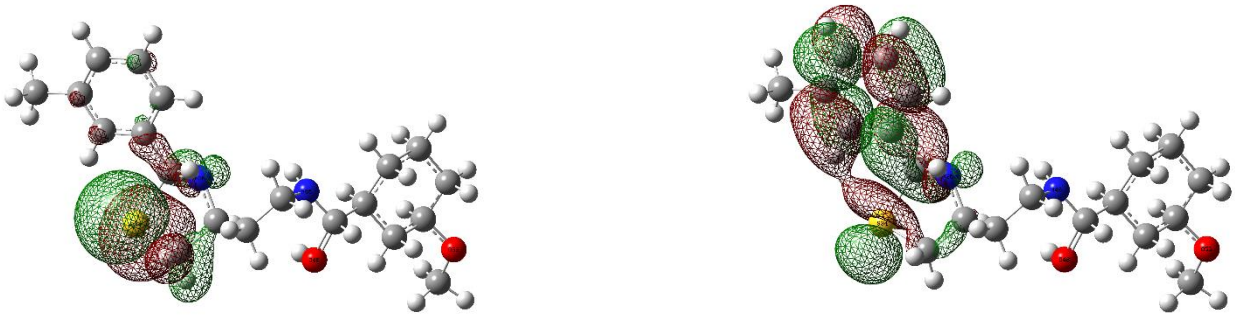

Fig 24: Frontier molecular orbital of compound 31802 (DIX domain of AXIN)

4.7 Molecular Dynamic Simulation

Further protein ligand interaction was investigated through molecular dynamics simulation to study the structural stability, the hydrogen bonding and total NAMD energy plot. For comparative analysis, the structural stability of the of PORCN bound with ligand 42151 were investigated by calculating the root mean square deviation (RMSD) that demonstrate the possible fluctuation from the backbone of the macromolecule.

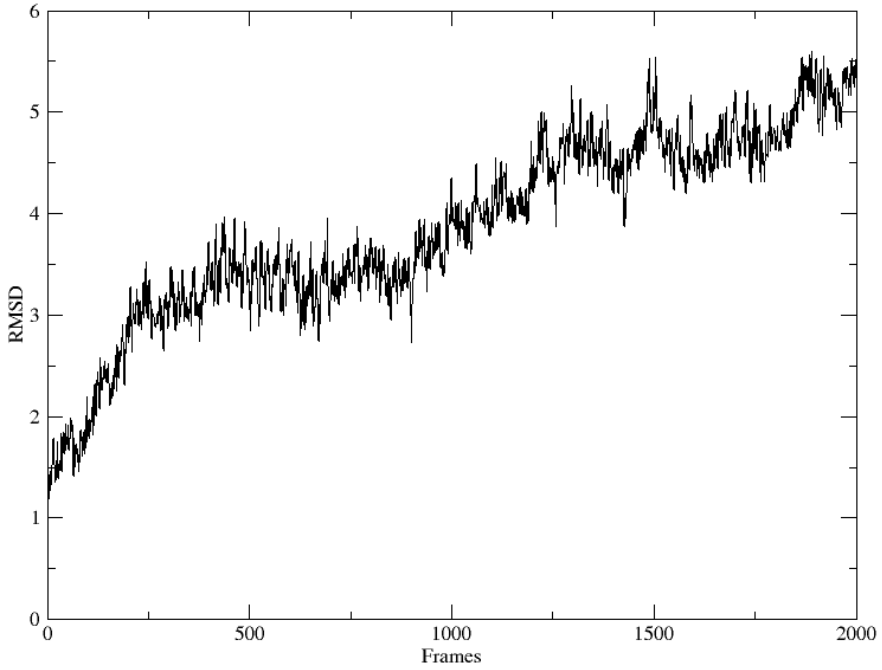

Fig 25: RMSD of protein PORCN and potential lead (42151) complex computed in 100ns production run.

Furthermore, we investigated the strength of hydrogen bonding between protein and ligand. During 100ns production run a total of 9 hydrogen bonds were seen interacting between the protein and ligand, which is listed in table

Table 16: H-bond between the protein and ligand during the course of 100ns simulation of the complex.

H-Donor	H-Acceptor
UNK1-Side	TYR329-Side
UNK1-Side	ASN309-Side
THR353-Side	UNK1-Side
UNK1-Side	SER332-Side
UNK1-Side	THR298-Side
THR328-Side	UNK1-Side
SER332-Side	UNK1-Side
SER292-Side	UNK1-Side
UNK1-Side	VAL297-Main

The plot illustrates fluctuations in the total energy of the system, indicating changes in energy states over time. Peaks and valleys suggest conformational changes, binding events, or interactions between the protein and ligand. Stability in energy denotes equilibrium, while sharp variations may signify dynamic processes. Sudden drops or rises in energy could indicate binding events or conformational rearrangements, respectively**.**

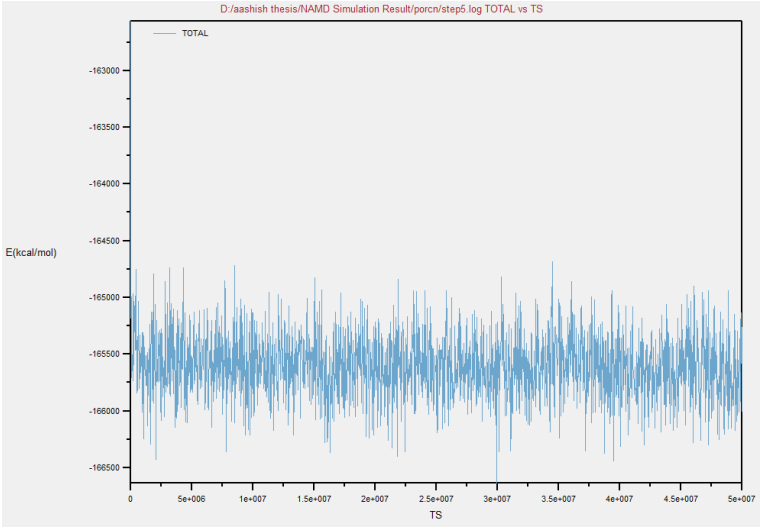

Fig 26: NAMD total energy plot of the protein ligand complex of PORCN and ligand 42151

Thus, the results of molecular docking, protein ligand interaction chimera and Bovia Discovery studio describes the bond nature and respective moieties of the ligand and amino acids involved for further analyzing pharmaceutical potential of the ligand against the target protein. Moreover, molecular dynamics (MD) simulations explain the stability of the interaction between the ligand and the protein in time scale and combining the results of both works would

support in subsequent analysis of the ligand molecule for their stability, reactivity and comparative pharmaceutical potential of the narrowed ligands.

CHAPTER 5

SUMMARY

These findings strongly indicate that computer-aided drug design (CADD) serves as a valuable tool for identifying potential lead compounds to combat multi-drug resistant pathogens. By screening a library of ligands according to the Lipinsky rule of five, candidates are refined for their drug-like properties, in addition to assessing ADME/Toxicity factors such as toxicity, mutagenicity, carcinogenicity, and teratogenic potential. Furthermore, additional screening using molecular docking against hMAT1A (PDB ID: 6SW5) aims to exclude compounds with stronger binding affinity than the native ligand SAM, as this could potentially compromise hepatic health. Given that many drugs are metabolized in the liver through phase I and phase II drug-metabolizing enzymes, particular attention is paid to Cytochrome P450s (Stavropoulou et al., 2018). Such narrowed ligands could be now screened for binding energy towards the target protein ligand binding active site through molecular docking. Such narrowed ligand with further comparative analysis with the total energy, its dipole moment, RMSD and energy gap was further screend into narrow range. With the comparataive analysis of binding of screened ligands with hMAT1A, hCYP3A4, phase I drug metabolizing enzymes, PI and DFT analysis, one or two potential lead compounds were screend/ such potential lead cpompounds could then be explored for protein ligand interaction. Additionally, the stability of protein-ligand interactions can be assessed using molecular dynamics, prioritizing ligands with more stable interactions for further investigation. Furthermore, ligands showing potential pharmaceutical efficacy can be analyzed for their inherent chemical properties, including various energies, to prioritize more reactive compounds.

CHAPTER 6

CONCLUSION

During this approach of drug discovery against disease associated with human is one of the very critical steps. With the development of etiological pathway PORCN, DVL and AXIN protein roles was found in more resonance with that of uterine fibroids, aromatase expression and over expression of estrogen hormone, which have caused female to experience menorrhagia as a disorder, hampering their social, economic life with great negative effect. From this study and the result obtained of molecular docking, protein ligand interaction, molecular dynamics analysis and Gausian analysis for the intrinsic chemical characteristics of the narrowed ligands revealed compounds 42151 (biogenic), compound 31802, compound 1765, compound 6736 and compound 31802 were one of the favored potential lead compound in maintaining the overexpression of estrogen by regulation the cellular proliferation, and expression of aromatase, a rate limiting enzyme in production of estrogen. Thereby, regulating uterine fibroids and thus menorrhagia.

CHAPTER 7

REFERENCE

Anandakrishnan, R., Aguilar, B., & Onufriev, A. V. (2012). H++ 3.0: automating pK prediction and the preparation of biomolecular structures for atomistic molecular modeling and simulations. Nucleic acids research, 40(Web Server issue), W537–W541. https://doi.org/10.1093/nar/gks375

Athanasiadis, E., Cournia, Z., & Spyrou, G. (2012). ChemBioServer: a web-based pipeline for filtering, clustering and visualization of chemical compounds used in drug discovery. Bioinformatics (Oxford, England), 28(22), 3002–3003. https://doi.org/10.1093/bioinformatics/bts551

Carpenter, K. A., Cohen, D. S., Jarrell, J. T., & Huang, X. (2018). Deep learning and virtual drug screening. Future medicinal chemistry, 10(21), 2557–2567. https://doi.org/10.4155/fmc-2018-0314

Chien, AJ., Lai, SL., Moon, RT. (2009). Wnt/Fz signaling and the cytoskeleton: potential roles in tumorigenesis. *Cell Res.*, *19*, 532-45.

Decherchi, S., & Cavalli, A. (2020). Thermodynamics and Kinetics of Drug-Target Binding by Molecular Simulation. Chemical Reviews, 120(23), 12788–12833. https://doi.org/10.1021/acs.chemrev.0c00534

Dolinsky, T. J., Czodrowski, P., Li, H., Nielsen, J. E., Jensen, J. H., Klebe, G., & Baker, N. A. (2007). PDB2PQR: expanding and upgrading automated preparation of biomolecular structures for molecular simulations. Nucleic acids research, 35(Web Server issue), W522–W525. https://doi.org/10.1093/nar/gkm276

Douguet D. (2010). e-LEA3D: a computational-aided drug design web server. Nucleic acids research, 38(Web Server issue), W615–W621. https://doi.org/10.1093/nar/gkq322

Dutkiewicz, Z., & Mikstacka, R. (2018). Structure-Based Drug Design for Cytochrome P450 Family 1 Inhibitors. Bioinorganic chemistry and applications, 2018, 3924608. https://doi.org/10.1155/2018/3924608

Ewing, T. J., Makino, S., Skillman, A. G., & Kuntz, I. D. (2001). DOCK 4.0: search strategies for automated molecular docking of flexible molecule databases. Journal of computer-aided molecular design, 15(5), 411–428. https://doi.org/10.1023/a:1011115820450

Friesner, R. A., Banks, J. L., Murphy, R. B., Halgren, T. A., Klicic, J. J., Mainz, D. T., Repasky, M. P., Knoll, E. H., Shelley, M., Perry, J. K., Shaw, D. E., Francis, P., & Shenkin, P. S. (2004). Glide: a new approach for rapid, accurate docking and scoring. 1. Method and assessment of docking accuracy. Journal of medicinal chemistry, 47(7), 1739–1749. https://doi.org/10.1021/jm0306430

Hall, A., Schlessinger, K., Tolwinski, N. (2009). Wnt signaling pathways meet Rho GTPases. *Genes Dev., 23*, 265-77.

Hamza, A., Wei, N. N., & Zhan, C. G. (2012). Ligand-based virtual screening approach using a new scoring function. Journal of chemical information and modeling, 52(4), 963–974. https://doi.org/10.1021/ci200617d

Herr, P., Basler, K. (2012). Porcupine-mediated lipidation is required for Wnt recognition by Wls. *Dev. Biol., 361*, 392-402.

Hughes, J. D., Blagg, J., Price, D. A., Bailey, S., Decrescenzo, G. A., Devraj, R. V., Ellsworth, E., Fobian, Y. M., Gibbs, M. E., Gilles, R. W., Greene, N., Huang, E., Krieger-Burke, T., Loesel, J., Wager, T., Whiteley, L., & Zhang, Y. (2008). Physiochemical drug properties associated with in vivo toxicological outcomes. Bioorganic & medicinal chemistry letters, 18(17), 4872–4875. https://doi.org/10.1016/j.bmcl.2008.07.071

Izumi, S., Kurayoshi, M., Kikuchi, A., Yamamoto, H. (2007). Post-translational palmitoylation and glycosylation of Wnt-5a are necessary for its signalling. *Biochem. J., 402*, 515-23.

Jegerschöld, C., Pawelzik, S. C., Purhonen, P., Bhakat, P., Gheorghe, K. R., Gyobu, N., Mitsuoka, K., Morgenstern, R., Jakobsson, P. J., & Hebert, H. (2008). Structural basis for induced formation of the inflammatory mediator prostaglandin E2. Proceedings of the National Academy of Sciences of the United States of America, 105(32), 11110–11115. https://doi.org/10.1073/pnas.0802894105

Jho, EH., Kim, W., Kim, M. (2013). Wnt/?-catenin signalling: from plasma membrane to nucleus. *Biochem. J., 450*, 9-21.

John, S., Thangapandian, S., Sakkiah, S., & Lee, K. W. (2011). Discovery of potential pancreatic cholesterol esterase inhibitors using pharmacophore modelling, virtual screening, and optimization studies. Journal of enzyme inhibition and medicinal chemistry, 26(4), 535–545. https://doi.org/10.3109/14756366.2010.535795

Kalliokoski, T., Salo, H. S., Lahtela-Kakkonen, M., & Poso, A. (2009). The effect of ligand-based tautomer and protomer prediction on structure-based virtual screening. Journal of chemical information and modeling, 49(12), 2742–2748. https://doi.org/10.1021/ci900364w

Kerns, E.H., Di L. (2009) Concepts, Structure Design and Methods from ADME to Toxicity Optimization. 1. *Academic Press*; Drug-like Properties

Kikuchi, A., Komekado, H., Yamamoto, H., Chiba, T. (2007). Glycosylation and palmitoylation of Wnt-3a are coupled to produce an active form of Wnt-3a. *Genes Cells, 12*, 521-34.

Köppen H. (2009). Virtual screening - what does it give us?. Current opinion in drug discovery & development, 12(3), 397–407.

Kühl, M., Rao, TP. (2010). An updated overview on Wnt signaling pathways: a prelude for more. *Circ. Res., 106*, 1798-806.

Kuntz, I. D., Blaney, J. M., Oatley, S. J., Langridge, R., & Ferrin, T. E. (1982). A geometric approach to macromolecule-ligand interactions. Journal of molecular biology, 161(2), 269–288. https://doi.org/10.1016/0022-2836(82)90153-x

Kurata, T., Satomi, Y., Kondoh, H., Takada, R., Takada, S., Takao, T. et al. (2006). Monounsaturated fatty acid modification of Wnt protein: its role in Wnt secretion. Dev. Cell, 11, 791-801.

Kurata, T., Satomi, Y., Kondoh, H., Takada, R., Takada, S., Takao, T. et al. (2006). Monounsaturated fatty acid modification of Wnt protein: its role in Wnt secretion. *Dev. Cell, 11*, 791-801.

Lavecchia, A., & Di Giovanni, C. (2013). Virtual screening strategies in drug discovery: a critical review. Current medicinal chemistry, 20(23), 2839–2860. https://doi.org/10.2174/09298673113209990001

Le Guilloux, V., Schmidtke, P., & Tuffery, P. (2009). Fpocket: an open source platform for ligand pocket detection. BMC bioinformatics, 10, 168. https://doi.org/10.1186/1471-2105-10-168

Leelananda, S. P., & Lindert, S. (2016). Computational methods in drug discovery. Beilstein journal of organic chemistry, 12, 2694–2718. https://doi.org/10.3762/bjoc.12.267

Lionta, E., Spyrou, G., Vassilatis, D. K., & Cournia, Z. (2014). Structure-based virtual screening for drug discovery: principles, applications and recent advances. Current topics in medicinal chemistry, 14(16), 1923–1938. https://doi.org/10.2174/1568026614666140929124445

Lipinski, C. A., Lombardo, F., Dominy, B. W., & Feeney, P. J. (2001). Experimental and computational approaches to estimate solubility and permeability in drug discovery and development settings. Advanced drug delivery reviews, 46(1-3), 3–26. https://doi.org/10.1016/s0169-409x(00)00129-0

Liu, S., Alnammi, M., Ericksen, S. S., Voter, A. F., Ananiev, G. E., Keck, J. L., Hoffmann, F. M., Wildman, S. A., & Gitter, A. (2019). Practical Model Selection for Prospective Virtual Screening. Journal of chemical information and modeling, 59(1), 282–293. https://doi.org/10.1021/acs.jcim.8b00363

Luga, V., Wrana, JL., Inanlou, MR., Chiu, E., Viloria-Petit, AM., Buchanan, M. et al. (2012). Exosomes mediate stromal mobilization of autocrine Wnt-PCP signaling in breast cancer cell migration. Cell, 151, 1542-56.

Luga, V., Wrana, JL., Inanlou, MR., Chiu, E., Viloria-Petit, AM., Buchanan, M. et al. (2012). Exosomes mediate stromal mobilization of autocrine Wnt-PCP signaling in breast cancer cell migration. *Cell, 151*, 1542-56.

Macalino, S. J., Gosu, V., Hong, S., & Choi, S. (2015). Role of computer-aided drug design in modern drug discovery. Archives of pharmacal research, 38(9), 1686–1701. https://doi.org/10.1007/s12272-015-0640-5

MacDonald, BT., Tamai, K., He, X. (2009). Wnt/beta-catenin signaling: components, mechanisms, and diseases. *Dev Cell*, *17*, 9-26.

Maia, E., Assis, L. C., de Oliveira, T. A., da Silva, A. M., & Taranto, A. G. (2020). Structure-Based Virtual Screening: From Classical to Artificial Intelligence. Frontiers in chemistry, 8, 343. https://doi.org/10.3389/fchem.2020.00343

McMahon, JA., Papkoff, J., McMahon, AP., Smolich, BD. (1993). Wnt family proteins are secreted and associated with the cell surface. *Mol. Biol. Cell*, *4*, 1267-75.

Michel, J., Tirado-Rives, J., & Jorgensen, W. L. (2009). Prediction of the water content in protein binding sites. The journal of physical chemistry. B, 113(40), 13337–13346. https://doi.org/10.1021/jp9047456

Morris, G. M., Huey, R., Lindstrom, W., Sanner, M. F., Belew, R. K., Goodsell, D. S., & Olson, A. J. (2009). AutoDock4 and AutoDockTools4: Automated docking with selective receptor flexibility. Journal of computational chemistry, 30(16), 2785–2791. https://doi.org/10.1002/jcc.21256

Ngan, C. H., Bohnuud, T., Mottarella, S. E., Beglov, D., Villar, E. A., Hall, D. R., Kozakov, D., & Vajda, S. (2012). FTMAP: extended protein mapping with user-selected probe molecules. Nucleic acids research, 40(Web Server issue), W271–W275. https://doi.org/10.1093/nar/gks441

Nunes, R. R., Fonseca, A., Pinto, A., Maia, E., Silva, A., Varotti, F. P., & Taranto, A. G. (2019). Brazilian malaria molecular targets (BraMMT): selected receptors for virtual high-throughput screening experiments. Memorias do Instituto Oswaldo Cruz, 114, e180465. https://doi.org/10.1590/0074-02760180465

Oishi, I., Minami, Y., Endo, M., Nishita, M. (2010). Ror-family receptor tyrosine kinases in noncanonical Wnt signaling:their implications in developmental morphogenesis and human diseases. *Dev. Dyn.*, *239*, 1-15.

Pfeffer, M. (1975). Drug Metabolism Reviews. Journal of Pharmaceutical Sciences, 64(10), 1735. https://doi.org/10.1002/jps.2600641045

Pinzi, L., & Rastelli, G. (2019). Molecular Docking: Shifting Paradigms in Drug Discovery. International journal of molecular sciences, 20(18), 4331. https://doi.org/10.3390/ijms20184331

Rai, B. K., Tawa, G. J., Katz, A. H., & Humblet, C. (2010). Modeling G protein-coupled receptors for structure-based drug discovery using low-frequency normal modes for refinement of homology models: application to H3 antagonists. Proteins, 78(2), 457–473. https://doi.org/10.1002/prot.22571

Rarey, M., Kramer, B., Lengauer, T., & Klebe, G. (1996). A fast flexible docking method using an incremental construction algorithm. Journal of molecular biology, 261(3), 470–489. https://doi.org/10.1006/jmbi.1996.0477

Reddy, A. S., Pati, S. P., Kumar, P. P., Pradeep, H. N., & Sastry, G. N. (2007). Virtual screening in drug discovery -- a computational perspective. Current protein & peptide science, 8(4), 329–351. https://doi.org/10.2174/138920307781369427

Rees, M. (1987). Menorrhagia. British Medical Journal (Clinical Research Ed.), 294(6574), 759–762. https://doi.org/10.1136/bmj.294.6574.759

Reya, T., Weissman, IL., Brown, JD., Yates, JR., Duncan, AW., Danenberg, E. et al. (2003). Wnt proteins are lipidmodified and can act as stem cell growth factors. *Nature, 423*, 448-52.

Rossant, J., Cox, BJ., Biechele, S. (2011). Porcupine homolog is required for canonical Wnt signaling and gastrulation in mouse embryos. Dev. Biol., 355, 275-85.

Rossant, J., Cox, BJ., Biechele, S. (2011). Porcupine homolog is required for canonical Wnt signaling and gastrulation in mouse embryos. *Dev. Biol., 355*, 275-85.

Sastry, G. M., Adzhigirey, M., Day, T., Annabhimoju, R., & Sherman, W. (2013). Protein and ligand preparation: parameters, protocols, and influence on virtual screening enrichments. Journal of computer-aided molecular design, 27(3), 221–234. https://doi.org/10.1007/s10822-013-9644-8

Seco, J., Luque, F. J., & Barril, X. (2009). Binding site detection and druggability index from first principles. Journal of medicinal chemistry, 52(8), 2363–2371. https://doi.org/10.1021/jm801385d

Shozu, M., Murakami, K., & Inoue, M. (2004). Aromatase and Leiomyoma of the Uterus. Seminars in Reproductive Medicine, 22(1), 51–60. https://doi.org/10.1055/s-2004-823027

Sliwoski, G., Kothiwale, S., Meiler, J., & Lowe, E. W., Jr (2013). Computational methods in drug discovery. Pharmacological reviews, 66(1), 334–395. https://doi.org/10.1124/pr.112.007336

Song, C. M., Lim, S. J., & Tong, J. C. (2009). Recent advances in computer-aided drug design. Briefings in bioinformatics, 10(5), 579–591. https://doi.org/10.1093/bib/bbp023

ten Brink, T., & Exner, T. E. (2010). pK(a) based protonation states and microspecies for protein-ligand docking. Journal of computer-aided molecular design, 24(11), 935–942. https://doi.org/10.1007/s10822-010-9385-x

Thomas, C., Garcia, KC., Waghray, D., Levin, AM., Janda, CY. (2012). Structural basis of Wnt recognition by Frizzled. Science, 337, 59-64.

Thomas, C., Garcia, KC., Waghray, D., Levin, AM., Janda, CY. (2012). Structural basis of Wnt recognition by Frizzled. *Science, 337*, 59-64.

Tresadern, G., Bemporad, D., & Howe, T. (2009). A comparison of ligand based virtual screening methods and application to corticotropin releasing factor 1 receptor. Journal of molecular graphics & modelling, 27(8), 860–870. https://doi.org/10.1016/j.jmgm.2009.01.003

Veber, D. F., Johnson, S. R., Cheng, H. Y., Smith, B. R., Ward, K. W., & Kopple, K. D. (2002). Molecular properties that influence the oral bioavailability of drug candidates. Journal of medicinal chemistry, 45(12), 2615–2623. https://doi.org/10.1021/jm020017n

Wang, X., Wallace, HA., Page-McCaw, A., Lee, E., Thorne, CA., Chen, TW. et al. (2013). The way Wnt works: Components and mechanism. *Growth Factors, 31*, 1-31.

Wang, X., Wallace, HA., Page-McCaw, A., Lee, E., Thorne, CA., Chen, TW. et al. (2013). The way Wnt works: Components and mechanism. Growth Factors, 31, 1-31.

Wang, X., Wallace, HA., Page-McCaw, A., Lee, E., Thorne, CA., Chen, TW. et al. (2013). The way Wnt works: Components and mechanism. *Growth Factors, 31*, 1-31.

Wang, X., Wallace, HA., Page-McCaw, A., Lee, E., Thorne, CA., Chen, TW. et al. (2013). The way Wnt works: Components and mechanism. *Growth Factors, 31*, 1-31.

Young, T., Abel, R., Kim, B., Berne, B. J., & Friesner, R. A. (2007). Motifs for molecular recognition exploiting hydrophobic enclosure in protein-ligand binding. Proceedings of the National Academy of Sciences of the United States of America, 104(3), 808–813. https://doi.org/10.1073/pnas.0610202104

Zhang, M. Q., & Wilkinson, B. (2007). Drug discovery beyond the 'rule-of-five'. Current opinion in biotechnology, 18(6), 478–488. https://doi.org/10.1016/j.copbio.2007.10.005

CHAPTER 8

APPENDICES

8.1 Active binding sites and docking coordinates of hMAT1A

Protein	Native Ligand	Active Sites		Coordinates		Binding energy
				Center	Dimension	(kcal/mol)
hMAT1A (Chain A and B)	S-adenosyl methionine(SAM)	Ala 55 Glu 70 Gln 112 Gln 113 Ser 114	Ile 117 Gly 133 Lys 289 Asp 291	X = 31.096 Y = -0.571 Z = 24.983	X = 27.625 Y = 57.151 Z = 32.622	-7.2

8.2 Active binding sites and docking coordinates of CYP3A4

Protein	Native Ligand	Active Sites		Coordinates		Binding energy
				Center	Dimension	(kcal/mol)
CYP3A4 (Chain A)	Ritonavir (RIT))	Tyr 53 Phe 57 Asp 76 Arg 105 Arg 106 Phe 108 Met 114 Ser 119 Ile 120 Leu 210 Leu 211 Phe 213 Phe 215 Thr 224 Phe 241	Ile 300 Ile 301 Phe 304 Ala 305 Thr 309 Ile 369 Ala 370 Met 371 Arg 372 Leu 373 Glu 374 Cys 442 Gly 481 Leu 482	X = 23.819 Y = - 30.303 Z = - 19.366	X = 28.368 Y = 28.403 Z = 26.540	-10.4

8.3 Active binding sites and docking coordinates of PORCN

Protein	Native inhibitor	Binding energy (Kcal/mol)	Active Sites		Coordinates	
					Center	Dimension
PORCN	050	-11.9	246 247 296 297 298 300 304 305 308 309 313 325	328 329 332 336 342 345 346 349 405 408 409 412	X= 113.588 Y= 107.081 Z= 106.739	X= 30.111 Y= 24.215 Z= 22.963

8.4 Active binding sites and docking coordinates of PDZ domain of DVL

Protein	Native inhibitor	Binding energy	Active Sites		Coordinates	
					Center	Dimension
PDZ domain of DVL	Sulindac		Phe 14 Leu 15 Gly 16 Ile 17 Ser 18 Ile 19 Val 20 Gly 21	Ser 35 Ile 36 Met 37 Asp 68 Val 71 Leu 74 Arg 75 Val 78	X= -0.569 Y= -0.714 Z= -5.401	X= 25.443 Y= 21.961 Z= 14.423

8.5 Active binding sites and docking coordinates of DEP domain of DVL

Protein	Reference Inhibitor	Binding energy	Interacting Residues		Coordinates	
			Chain A	Chain B	Chain	Dimension
DEP domain of DVL (PDB: 5LNP)	Sulindac		Val 419 Leu 417 Ser 435 Gly 436 Arg 440 Asp 441 Met 443 Leu 445 Ile 447 Ala 452 Asn 451 Trp 461 Glu 467	Gly 467 Trp 461 Ala 452 Ile 449 Ile 447 Leu 445 Met 443 Arg 440 Asp 441 Ser 435 Leu 417 Val 419	X= -2.970 Y= 11.401 Z= -3.593	X= 53.934 Y= 26.564 Z= 60.967

8.6 Active binding sites and docking coordinates of DIX domain of DVL

Protein	Reference Inhibitor	Binding energy	Interacting Residues	Coordinates	
			Chain B	Chain	Dimension
DIX domain of DVL	XAV 939 E 7449 Longdaysin		Glu 23 Pro 26 Leu 28 Val 46 Leu 47	X= 61.402 Y= 68.666 Z= 14.555	X= 17.800 Y= 16.389 Z= 17.467

8.7 Active binding sites and docking coordinates of DIX domain of AXIN

Protein	Reference Inhibitor	Binding energy	Interacting Residues	Coordinates	
			Chain A	Chain	Dimension
DIX domain of AXIN	XAV 939 E 7449 Longdaysin		Lys 821 Phe 801 Glu 802 Glu 803 Arg 785	X= 63.114 Y= 63.624 Z= 18.725	X= 17.686 Y= 14.108 Z= 19.266

8.8 Active binding sites and docking coordinates of Phase I Drug metabolizing enzymes

Protein (PDB Id)	Reference Inhibitor	Binding Energy (Kcal/mole)	Active sites	Coordinates	
				Chain	Dimension
CYP1A1 (4I8V)	BHF	-14.3	115, 116, 120, 123, 222, 224, 255, 258, 312, 313, 316, 317, 319, 320, 321, 386, 496, 497, Hem 600	X= -13.7675	X= 22.8811
				Y= 87.0858	Y= 22.1685
				Z= -61.2303	Z= 22.2398
CYP1A2 (2HI4)	BHF	-14.7	117, 118, 122, 124, 125, 223, 226, 227, 256, 260, 312, 313, 316, 317, 320, 321, 382, 386, 497, 498, HEM 900	X= 3.5717	X= 25.3799
				Y= 17.5653	Y= 26.2844
				Z= 19.7810	Z= 23.1609
CYP1B1 (3PM0)	BHF	-14.6	126, 127, 131, 133, 134, 227, 228, 231, 264, 265, 268, 325, 326, 329, 330, 332, 333, 334, 399, 509, 510, HEM 900	X= -18.7083	X= 24.9154
				Y= 23.1374	Y= 28.4403
				Z= -19.6448	Z= 22.8482
CYP2C9 (1OG5)	SWF	-9.9	97 98 99 100 102 103 113 114 208 213 217 364 365 366 367 388 476 HEC	X= -20.2253	X= 25.3143
				Y= 84.6944	Y= 24.4768
				Z= 35.5935	Z= 27.4291
CYP2C19 (4GQS)	0XV	-9.8	113 114 205 208 293 296 297 300 301 362 366 476 477 HEM	X= -81.403	X= 22.428
				Y= 22.713	Y= 21.260
				Z= -42.187	Z= 19.667
CYP2D6 (4WNW)	RTZ	-9.8	110 112 120 121 208 209 212 213 216 244 247 248 297 300 301 304 305 308 309 370 373 374 484 483 HEM	X= -6.4685	X= 28.4950
				Y= -9.5409	Y= 27.7823
				Z= 30.7931	Z= 20.1539
CYP2E1 (3T3Z)	9PL	-7.3	103 106 115 116 207 210 298 299 302 303 364 368 437 478 HEM	X= 24.454	X= 21.146
				Y= 27.265	Y= 22.993
				Z= 12.960	Z= 22.198

8.9 Binding energy of Reference inhibitor of target protein with hMAT1A and hCYP3A4

Target Proteins	Reference Inhibitors	hMAT1A	hCYP3A4
PORCN	wnt-c59	**-9.5**	**-10.9**
	drug_wnt974	**-9.4**	**-10.4**
	lgk-974	**-9.6**	**-10**
DEP-DEP domain of DVL	sulindac_1548887	**-7.6**	-9.1
PDZ domain of DVL			
DIX domain of DVL	135418940_uff_e=264.96	**-7.8**	-8.5
	135565981_uff_e=348.38	**-8.8**	**-10.8**
DIX domain of AXIN	49830252_uff_e=323.48	**-8.1**	-8.8
	SAM and SAH (Native ligand)	**-7.2**	**-**
			-
	RITO	**-**	**-10.5**

final thesis_plagiarism_check_aashish_pokharel.pdf

ORIGINALITY REPORT

17%
SIMILARITY INDEX

HORMONAL HOMEOSTASIS TO MITIGATE FEMALE HORMONE DISORDER: A COMPUTATIONAL APPROACH

PRIMARY SOURCES

1	ftp.cbi.pku.edu.cn Internet	369 words — 2%
2	www.ncbi.nlm.nih.gov Internet	214 words — 1%
3	jhoonline.biomedcentral.com Internet	151 words — 1%
4	www.mdpi.com Internet	134 words — 1%
5	www.reactome.org Internet	110 words — 1%
6	elibrary.tucl.edu.np Internet	100 words — 1%
7	M. Habib Rahuman, S. Muthu, B.R. Raajaraman, M. Raja, H. Umamahesvari. "Investigations on 2-(4-Cyanophenylamino) acetic acid by FT-IR,FT-Raman, NMR and UV-Vis spectroscopy, DFT (NBO, HOMO-LUMO, MEP and Fukui function) and molecular docking studies", Heliyon, 2020 Crossref	88 words — < 1%
8	"Pharmacology of the WNT Signaling System", Springer Science and Business Media LLC, 2021 Crossref	83 words — < 1%